Treball de Fi de Màster

Màster Universitari en Enginyeria Industrial (MUEI)

Design and optimisation of the architecture and the orientation of utility-scale photovoltaic power plants

REPORT

Author: Eduard Foved Johe
Director: Oriol Gomis Bellmunt

Call: April 2019

Escola Tècnica Superior
d'Enginyeria Industrial de Barcelona

Abstract

The Spanish and European photovoltaic markets are set for a revival: massive GW deployments are expected in the coming years. Large utility-scale PV will increasingly take a role as baseload power plants, displacing dirtier sources of energy. PV project developers will need to optimise their design practices so as to achieve the most cost-effective solutions possible.

For all these reasons, the present work is focused on the development of utility-scale PV plants in the Spanish context.

A MATLAB based programme to simulate PV plants (developed by a former MSc Thesis student) has been improved and updated with new models, databases and performance indicators. Three main new models have been added to the original code: tracking system model, self-shading model and battery model.

The updated MATLAB programme has been used to simulate a 100 MWp PV plant in Seville, Spain. Several relevant topics have been studied: the selection between string and central inverters and their DC/AC ratio; the effect of including trackers; the effect of self-shading losses on land-use; and the inclusion of a battery to provide flat-output response.

Central inverters are found to be still more cost-effective, but string inverters follow the pace. DC/AC inverter ratios are concluded to be a fundamental designing choice impacting both performance and cost.

Tracker devices are found to be highly competitive solutions (depending on the location), but a more careful study on land-use will be required in future works.

A compromise in performance have been found between self-shading losses and land-use: reducing land-use reduces considerably the energy yield, thus row spacing and module configuration are fundamental design choices.

Batteries providing services to the grid will play a key role in renewable energy integration, such as the flat-output response studied. However, further battery cost reductions or government incentives are required to make these projects more profitable.

The PV industry and policy regulators must work together to ensure a sustainable development of the European and Spanish utility-scale PV sectors, with PV developers enhancing and refining their design best practices.

Table of contents

List of tables

List of figures

List of nomenclatures, abbreviations and terminologies

A_m: Module area

AC. Alternating Current

AOI: Angle Of Incidence

a-Si: Amorphous silicon

BNEF: Bloomberg New Energy Finance

BOS: Balance Of the System

CAPEX: Capital Expenditures

CdTe: Cadmium telluride

CIGS: Copper Indium Gallium (Di)Selenide

c-Si: Crystalline silicon

DC: Direct Current

DC/AC ratio: Inverter ratio at nominal capacities of the PV array and the inverter

DHI: Diffuse Horizontal Irradiance

DNI: Direct Normal Irradiance

DOD: Depth of discharge of the battery

E_i: component i of the POA irradiance

EPC: Engineering, Procurement, Construction

EUR: Euro (€)

E-W: East-West

FF: Fill Factor

g: shadow displacement

G_i: component i of the irradiance

GCR: Ground Coverage Ratio

GHI: Global Horizontal Irradiance

Hs: shadow height

IAM: Incidence Angle Modifier

IV curve: curve intensity-current of a photovoltaic module

L: Module height

LCOE: Levelized Cost of Electricity

LID: Light-Induced Degradation

MIP: Minimum Import Price

MLPE: Module Level Power Electronics

MPP: Maximum Power Point

NREL: National Renewable Energy Laboratory

OPEX: Operational Expenditures

PCC: Point of Common Coupling

PERC: Passivated Emitter and Rear Contact

POA: Plane Of Array

PPA: Power Purchase Agreement

PR: Performance Ratio

PV: Photovoltaic

p-type: semiconductor doped with acceptor impurities (boron)

R_{aspect}: Module aspect ratio

SAM: System Advisor Model

SOC: State of charge of the battery

SSF_i: Self-shading loss factor for the component i of the irradiance (or in the non-linear case for the DC output)

STC: Standard Test Conditions (a cell temperature of 25°C and an irradiance of 1000 W/m^2 with an air mass 1.5 (AM1.5) spectrum)

USD: US Dollar

W: Module width

W_p: Watt peak

1. Preface

1.1. Project origin

The present project follows the work started by Gabriele Catalano during his Master Thesis *"Development of a model to simulate solar PV plants in MATLAB with a study on the effects of under-sizing the inverter"* (2018) [1], within the research centre CITCEA from the Polytechnic University of Catalonia (UPC).

This project is intended to upgrade and update the existent models present in Gabriele Catalano's MATLAB code, as well as adding new models to enhance the simulation performance.

1.2. Motivation

The project follows the idea to provide the research centre CITCEA with a MATLAB programme to simulate photovoltaic plants. Three main reasons arise to justify this motivation:

- Providing a non-expensive (free) PV plants simulator programme;
- Providing a flexible, adaptable and easily tuneable tool to the researchers' desires;
- Providing an academic tool for students aiming to pursue a professional career in the renewables and solar sectors.

It is well known the existence of impressive and performant PV plants simulator programmes, such as PVsyst or SAM (NREL). However, the former is known to be an expensive software and the latter, while being free, it is not mainly intended to be flexible and modifiable by the users from a code point of view. Finally, the possibility to interact within the code with the physical models of the photovoltaic systems could provide students (and future PV professionals) with a precious understanding on the real behaviour and functioning of PV plants, which could be of great help in the fast-developing but still young solar industry.

1.3. Previous requirements

Good programming skills within MATLAB environment are required. In addition, a good understanding of the renewable energy and photovoltaic industry from a techno-economic point of view is desirable.

2. Introduction

2.1. Objectives

The main goal of this project is to continue improving and developing CITCEA's MATLAB programme for simulating photovoltaic power plants, a project started by the aforementioned Gabriele Catalano. The main models added to the programme will be:

- Inclusion of tracking devices;
- A model to consider self-shading losses due to adjacent rows;
- A model to allow the inclusion of batteries.

In addition, several minor changes and updates of the original code will be implemented, such as updates and expansions of the PV module database, the inverter database and the meteorological files; or the inclusion of other DC losses not previously considered. These minor changes are going to be commented in a special chapter in section 4.

Moreover, the resulting upgraded programme is going to be used in several cases studies, with the aim to analyse and to propose innovative solutions for utility-scale PV plants. The solutions will be focused on the architecture of the converters (string vs central inverters) and on the orientation towards the sun (south or E-W orientation, inclusion of trackers, etc.). The inclusion of batteries to provide grid services will also be studied. The different solutions will be designed, optimised and assessed considering technical, economic and terrain constraints criteria.

2.2. Scope of the project

The scope of this project covers the study, implementation and upgrades of a MATLAB programme to simulate the behaviour of photovoltaic power plants from irradiance to AC electricity (until the point of common coupling, PCC). Moreover, techno-economic analysis with financial metrics such as the LCOE (Levelized Cost of Electricity) are also within the scope of the present project.

On the other hand, the development of a self-shading model is restricted to fixed surfaces with no tracking. The self-shading model for one-axis tracking is not enabled, since it is required to develop a new, different and complex model not worth to invest the effort in it (a typical self-shading model for 1-axis tracking PV systems can be consulted in SAM documentation [2]). It is important to remark that the tracking model has been developed to assess its advantages/disadvantages with respect to systems with no tracking, thus simulating both

systems without self-shading losses will provide a quite accurate comparison.

Regarding the PV technologies studied, a main focus is given to crystalline silicon solar cells. The programme also allows the selection of thin-film technologies within its database (CdTe, CIGS and a-Si).

In addition, an extra consideration needs to be given when selecting CdTe modules: both PVsyst [3] and First Solar [4] (the most important CdTe module manufacturer) suggest that a spectral correction is required to simulate accurately this technology (especially in high humidity environments). Nevertheless, since the great majority of PV projects (as well as the case studies of this project) choose c-Si technologies and given the fact that the error induced when avoiding these corrections is not remarkable for this project; the development of a model to correct the spectral irradiance for CdTe technology is out of the scope of this project.

Finally, the simulation of batteries providing services to the grid, the model chosen is restricted to a flat-output response, a very interesting battery purpose allowing predictable PV outputs.

2.3. Structure

The present work is structured in the following way:

- Firstly, section 3 introduces the reader to photovoltaic energy and its markets, as well as in the particular case of the Spanish market.
- Secondly, section 4 focuses on explaining the characteristics and particularities of the existent PV simulation MATLAB programme; and then continues with the explanation of the new models included (tracking, self-shading and battery models; and the inclusion or improvement of other submodels).
- Thirdly, section 5 performs a validation of the main models added to the MATLAB code.
- Finally, the improved MATLAB code is used to perform simulations to analyse several case studies.

In addition, the project also includes several sections at the end with a focus on the planning of a PV project, a summary of the associated costs and its environmental impacts.

The document ends with a conclusions section stating the main outcomes of this work.

3. General photovoltaic context

This section aims to provide the reader with a context on photovoltaic energy, which will highlight why this thesis is focused on this kind of renewable energy.

Firstly, a first chapter explaining briefly the story of photovoltaic energy is presented (chapter 3.1). This chapter is then followed by the facts that explain the increased importance of PV: improvements in costs and efficiency (chapter 3.2). A brief explanation of commercial PV technologies is also included (chapter 3.3). Finally, two extra chapter are included due to important relevance in the present work: the Spanish solar renaissance (chapter 3.4) and the coupling of PV installations with batteries (chapter 3.5).

3.1. Brief story of photovoltaic energy

The start point of photovoltaic energy is located in the 19th century: Antoine and Alexandre Edmond Becquerel discovered the photoelectric effect in 1839 [5], later explained by Albert Einstein in 1905, who was awarded a Nobel prize for it. Photovoltaic cells use this effect to generate DC electricity from solar irradiance [6].

However, it is not possible to find a real application for PV cells until the 1960s: electricity supply for satellites, just when the space race started. Thus, PV cells were seen as a product for niche markets. In fact, the market being currently dominated by p-type products (mono or multi crystalline) is also a consequence of the space race: p-type wafers are much more resistant to the harsh space irradiance and conditions.

Nevertheless, as it happened in many industries before, innovation and cost-performance improvements brought this niche technology to other markets: from autonomous and remote applications in need of a reliable energy supply; to the conquest of the whole energy industry, a process that is in the making.

Recent news state that last year worldwide PV installation topped a new record of 104 GW, meaning that the current online PV capacity is greater than 500 GW [7]. These numbers take special relevance when considering the events that occurred in June 2018: the Chinese government drastically cut off subsidies to solar energy, which in turn produced a stagnation in Chinese solar deploys (from installing 53 GW in 2017 [8] to 44 GW in 2018 [9]). However, even if the largest PV market (China) suffered due to changes in subsidy policies, the global market still increased 2017 PV installations (from 100 GW to the above-mentioned 104 GW). The reason is simple, cut off in Chinese installations produced an oversupply of PV modules (since China is also the main player in PV manufacturing). The oversupply led to an abrupt

drop in prices (up to 34% as stated by Bloomberg New Energy Finance [10]), encouraging other non-Chinese regions to accelerate their solar deployments. Within these regions, the European Union was especially favoured by the end of the minimum import price (MIP) on Chinese PV modules [11], which made prices decrease even more abruptly.

3.2. The enablers of the photovoltaic success story: cost and efficiency

The explanation of this starting PV success story has its roots in its competitive electricity production costs. The main indicator for the electricity production costs can be found in the levelized cost of electricity (LCOE), which is an economic assessment that allows comparing different power plants or even sources of energy on a comparable basis. In addition, its value can also be seen as the minimum price at which energy/electricity should be sold in order to break-even during the lifetime of the project. Its calculation will be explained detail in section 6. Next figure shows the evolution of LCOE for PV installations in different countries:

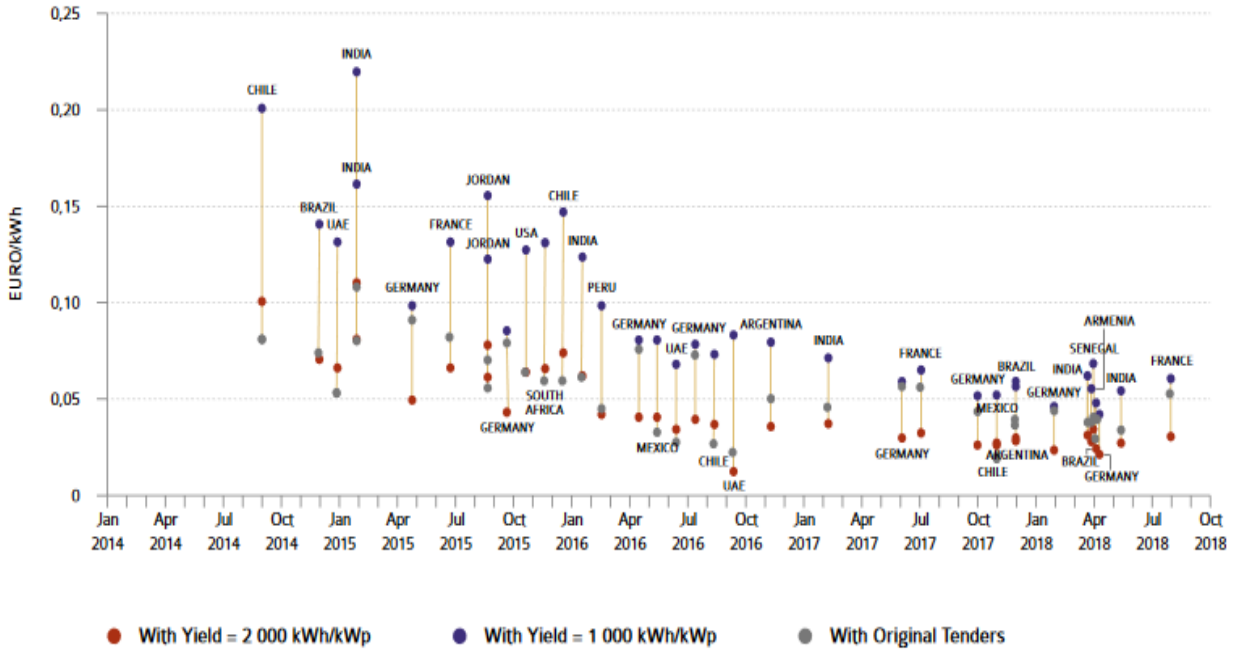

Figure 1. PV LCOE evolution (2014-2018) for different countries and under different conditions for yield or considering the tender final price. Source: IEA PVPS [12].

As it can be observed in Figure 1, PV LCOE has evolved from around 0,1-0,2 EUR/kWh (2014) to values lower than 0,05 EUR/kWh (2018), which is the same to say that PV has reached values of LCOE lower than 50 EUR/MWh worldwide. The competitiveness of these values can be further assessed when compared with the LCOE of other sources of energies: according

to a report published by Lazard in November 2018 [13], utility-scale PV is already the cheapest source of electricity in a LCOE basis. A report from Bloomberg New Energy Finance [14] also reaches the same conclusion, as seen in Figure 2:

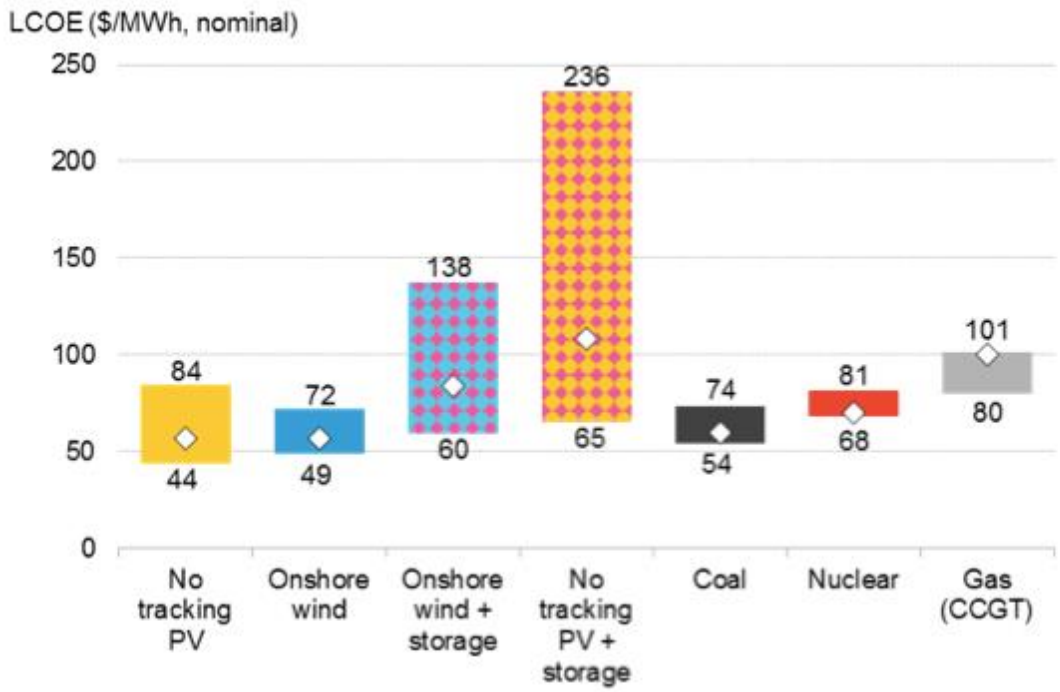

Figure 2. LCOE comparison between several renewable and conventional energy sources. Source: BNEF via PV magazine [14].

These astonishing low costs are led by two major improvements: equipment cost reduction and efficiency increases of PV technologies.

3.2.1. Equipment cost reduction

The two main components of PV power plants (modules and inverters) have suffered drastic price drops during the recent years. In fact, as stated by Bloomberg New Energy Finance, the benchmark CAPEX for a whole utility-scale fixed-axis PV system has decreased from 3,24 USD/W_p in 2010 to less than 1 USD/ W_p in 2018 [15].

Especially remarkable is the decrease in modules cost: current PV modules (2019) can cost as much as 17% of what they costed back in 2010 (1,85 USD/W_p in 2010 to less than 0,3 USD/ W_p in 2018). What explanation can be given to these data? Two interconnected answers arise: economies of scale and efficiency improvements.

Economies of scale in the PV industry can be easily summarised with the following graph:

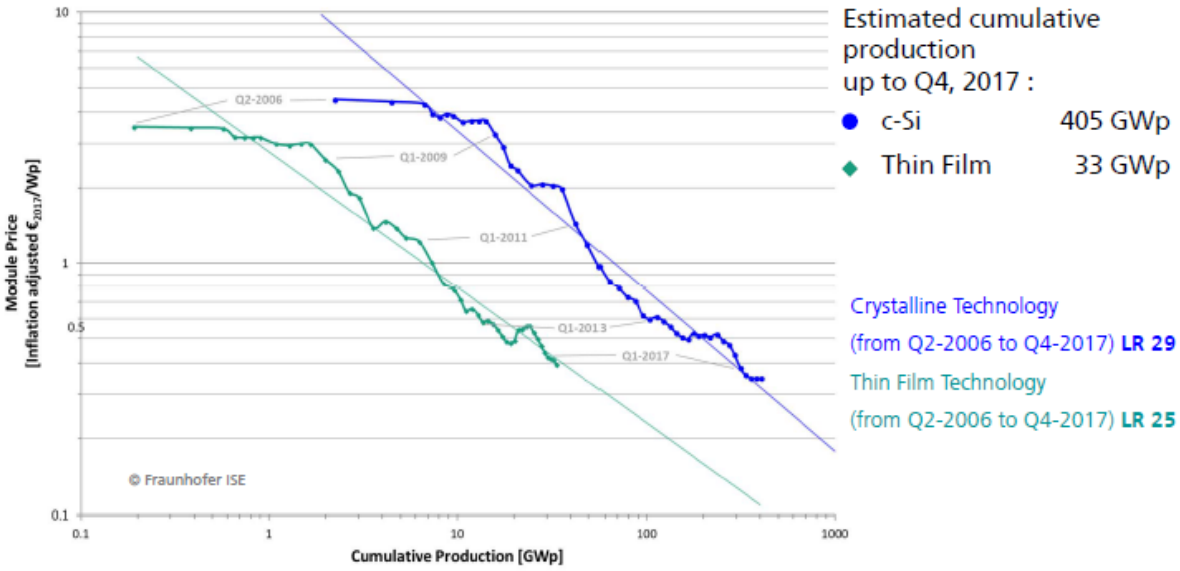

Figure 3. PV Price learning curve. Source: Fraunhofer ISE [16].

Figure 3 shows one of the most known graphics within the PV industry: the price learning curve. The graphic plots the different prices registered on PV technologies (crystalline silicon or thin-films) as a function of the global cumulative PV capacity at the time the price was registered. The graphic is plotted on a logarithmic scale.

The higher is the cumulative capacity, the lower is the price, showing perfectly the economies of scale effect.

But this is not the only conclusion that one can extract from this Figure 3. In fact, the price learning curve has been used to make really accurate predictions on future PV prices, since the data trends (shown by the two straight lines in the figure) provide a good estimation tool.

The third conclusion one can come up is the cost reduction potential of thin-films technologies. Despite not being the popular choice for PV plants (crystalline silicon steals the show), in the hypothetical case of having the same production capacity as c-Si, thin-films would be largely the cheapest technologies. The reason for that can be explained by lower raw material consumption and manufacturing processes that do not include CAPEX and energy intensive activities such as in c-Si.

However, the cost reduction push cannot be understood without commenting efficiency. A higher PV efficiency means a higher energy production for the same surface and normally for the same quantity of raw materials. If this increased energy production compensates the consequential added costs of increasing efficiency (new manufacturing tools or technologies, R&D, etc.), the result is a cost reduction on a euro per Watt peak basis (EUR/W_p). In the end,

a cost dilution is happening, more energy production (or more peak power of PV modules) dilutes the total costs.

3.2.2. PV efficiency increase

As commented in the previous lines, the efficiency increase is a key enabler in the photovoltaic success story. Next Figure 4 shows the recent lab efficiency evolution:

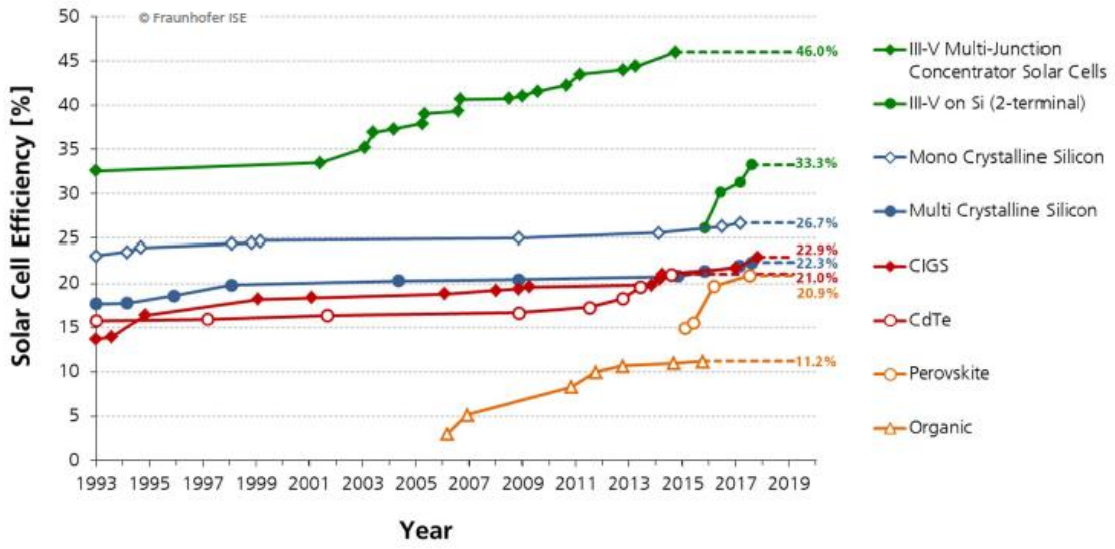

Figure 4. Evolution of lab solar cell efficiency. Source: Fraunhofer ISE [16].

As seen in Figure 4, solar cell efficiencies at a lab level have an increasing trend over the last 25 years. However, one could argue that the most popular technology (mono or multi c-Si, blue lines) have been suffering a stagnation period. Partly this reasoning is true, but only at a lab scale. It is true that the actual c-Si standard technology (PERC) was developed by University of New South Wales (UNSW) researchers 30 years ago [17], but the transfer of the technology to a commercial product has been a tough one. This means that, at a commercial level, module efficiencies have been increasing intensively during the last decade.

In fact, the c-Si lab cell efficiency record of 26,7% [18] is extremely close to the theoretical single junction efficiency limit of 29% for crystalline silicon (the Shockley-Queisser limit [19]). This is why PV researchers are searching for new ways to keep improving efficiency (and consequently diluting/reducing costs). The latest interest in PV research are tandem devices, two solar cells stacked together mechanically or electrically that allow overcoming the above-mentioned efficiency limit. Tandem devices combining silicon solar cells with other materials (such as perovskite) are on the rise.

3.3. Commercial PV technologies

This chapter has the objective to present briefly the main PV technologies deployed in PV projects.

As seen in last Figure 4, numerous PV technologies exist at a lab scale. However, few of them cross the bridge between research and market, understanding by market the PV projects market (excluding niche applications such as space exploration, calculators power supply, solar powered backpacks or small/remote PV applications). In fact, we can currently name three main technologies in this category:

- **Crystalline silicon (c-Si):** represents more than a 95% of the PV market [16]. The technology is based on silicon wafers (monocrystalline or multicrystalline wafers, depending on the number of silicon crystals), which then are transformed into cells. During the last year (2018), PERC (Passivated Emitter and Rear Contact) monocrystalline modules aroused as the dominant and new standard technology [20]. However, other cell technology concepts with higher efficiencies like the IBC (interdigitated back contact) or the heterojunction solar cells have still their own market in premium applications [20], with the aim to battle the beginning PERC dominance.
- **Cadmium telluride (CdTe):** probably the most commercial thin-film technology. Produced mostly by the American company First Solar [21], the technology seems ideal for large utility-scale power plants, since it has a superior relative performance in warm and humid weathers [22].
- **Copper Indium Gallium (Di)Selenide (CIGS):** always considered as a promising technology, CIGS has continuously suffered from a poor lab to market transfer (lab and cell efficiencies are impressive, but module efficiencies are significantly lower due to cell to module loss). Despite this, the technology is well appreciated in residential environment due to properties such as the possibility to make flexible modules. Traditionally, the Japanese manufacturer Solar Frontier dominated CIGS production [23], but recent Chinese investments such as Hanergy [24] can make an impact on the technology.

It is possible that some readers miss amorphous silicon (a-Si) in this summary, but the truth is that the technology that boomed in 2008 is right now obsolete and, in fact, a great number of a-Si manufacturers are upgrading their lines to other technologies [25].

3.4. The Spanish solar renaissance

Since this project's case studies are going to be focused on the Spanish solar context, this chapter presents the recent developments in the country concerning photovoltaic energy.

Spain was one of the first countries to bet heavily on solar energy. In fact, the country leaded the pace at an international level with almost 4,7 GW of capacity installed between 2006 and 2012 [26]. However, the significant effect of the economic crisis together with controversial decisions made by the Spanish government produced a stagnation in PV installations. Notably, the retroactive decision to cut already agreed feed-in tariffs decreased Spanish appeal through investors' eyes. Some international courts are even starting to rule against the retroactive decision, meaning that Spain will be forced to pay compensations [27].

Nevertheless, 2018 was a new beginning. The drastic drop in PV module prices together with a favourable environment to invest in the Spanish solar industry (an optimistic climate and a new government with "pro-solar" policies). The beginning of the Spanish solar renaissance has already started: 261,7 MW of new PV systems were installed in Spain during 2018, according to the Spanish solar energy association (UNEF), meaning that the country has already surpassed the 5 GW barrier of cumulative capacity [28].

But the best is yet to come: SolarPower Europe, the European solar energy association, forecasts that Spain will be the hottest European market in 2019, with new PV installations being able to reach GW scale (SolarPower Europe prospects a medium scenario of new PV installations of around 9 GW between 2019-2022) [29]. Moreover, this new solar wave is led by unsubsidised installations both in the form of public tenders (auctions) or private bilateral power purchase agreements (PPAs) [30] [31].

The awaken of the Spanish solar industry makes very interesting to locate the case studies of this project in Spain, the European country with the highest annual solar irradiation and now becoming the PV equivalent for "El Dorado" [32].

3.5. Coupling PV installations with batteries

Being solar PV an intermittent and variable source of electricity, dependent on weather conditions, the use of storage devices that can help integrating this variable generation takes an important relevance. Batteries are seen as one of the most promising storage systems suitable to be coupled to PV installations.

Batteries can provide services to the grid, such as frequency regulation or enhancement of power quality. They can also provide new business models to PV + battery plants owners,

since energy arbitrage could become a new source of income. And another possible use is to provide a more predictable energy output for renewable power plants, for instance, providing a flat-output for several hours as will be studied in this project.

Regarding battery technologies, it is true that there are many and different ones. However, lithium-ion batteries have established themselves as the dominant technology, partly because of the large cost reduction produced by its extensive use and development in the electric vehicle industry. Other promising battery technologies can arise through innovation, such as redox flow batteries, which seem ideal for large scale applications if they achieve important cost reductions [33].

Thus, batteries are expected to become a key player to ensure a good integration of photovoltaic power plants within the electricity grid. For this reason, a case study of a battery coupled to the PV plant providing a flat-output service is included in this work.

4. MATLAB model of the photovoltaic plant

The purposes of this section are stated in the following lines:

- To present, in a general way, the different parts of the MATLAB model, including the ones developed by Gabriele Catalano during his MSc Thesis [1];
- To present and explain in detail the new models included in the code during the development of the present project (tracking, self-shading and battery models);
- To present updates, changes and modifications introduced to the original code (but not considered as completely new models).

4.1. General view of the MATLAB model

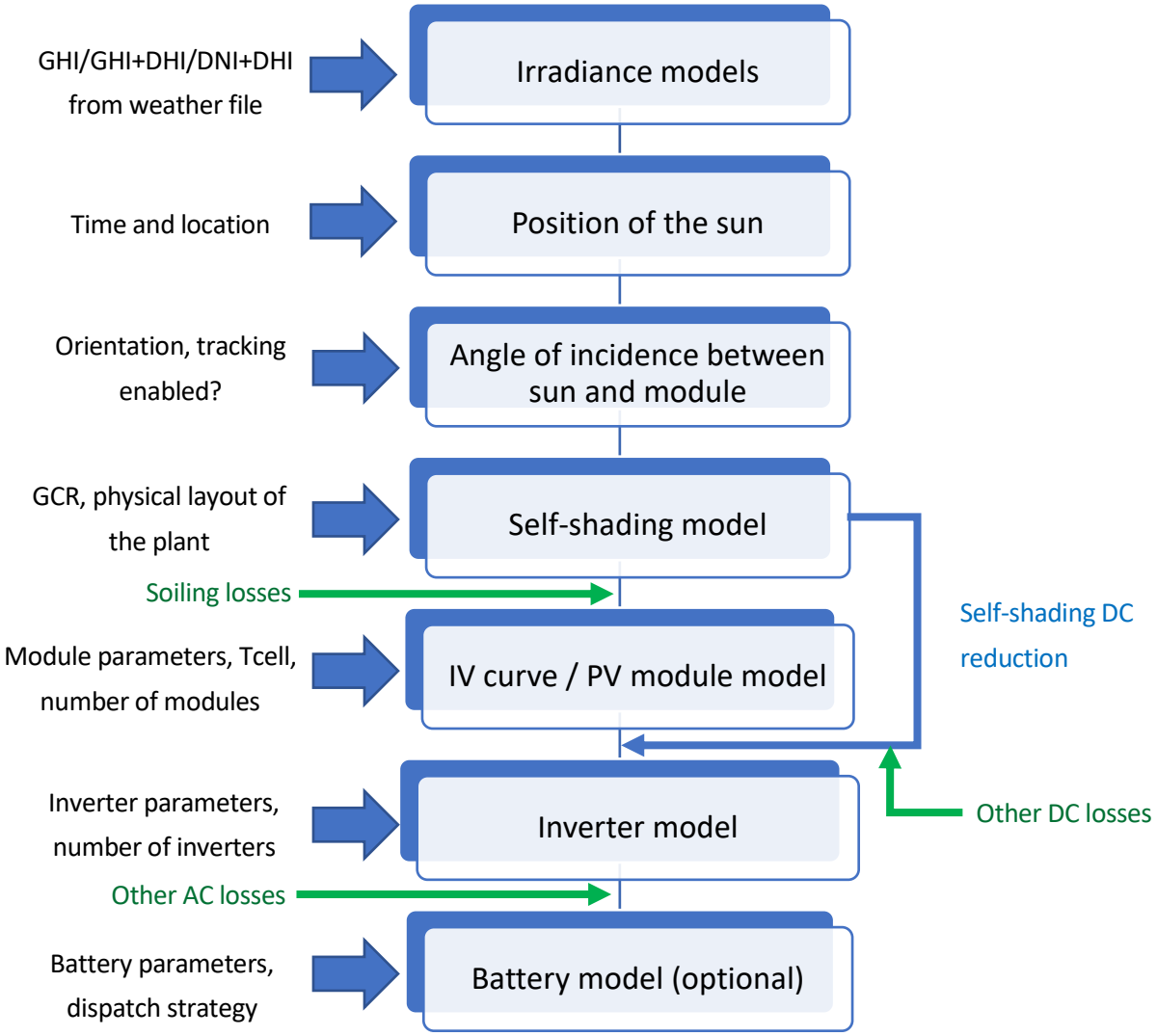

Figure 5. Schematic representation of the MATLAB model of the photovoltaic plant. Source: Own

Figure 5 presents the general scheme of the PV plant MATLAB model. The scheme shows the different building blocks corresponding to the physical and technical models included in the code. Be aware that these building blocks can group different sub-models within them, particularly when the sub-models are of the same topic and are used to achieve the final goal of their respective building blocks. In addition, the main external inputs needed for the completion of the simulations (indicated with the big blue arrows) and several factors for important losses (written in green and blue colours) are also shown in Figure 5.

Next lines will present the general insights on the MATLAB code. However, more precise information could be found in Gabriele Catalano's Master Thesis [1] or in the following chapters (for the models introduced in the present work).

The MATLAB model starts when introducing the hourly irradiance values for a whole year and for a specific location (coming from a weather file). The model allows introducing the irradiance in three different ways depending on its components available in the weather files:

- Global horizontal irradiance (GHI) and diffuse horizontal irradiance (DHI);
- Direct normal irradiance (DNI) and diffuse horizontal irradiance (DHI);
- Global horizontal irradiance (GHI), while estimating the and diffuse horizontal irradiance (DHI) by means of the Erb's correlation.

The next step of the model is calculating the sun position at any time for the location desired. The sun position is defined by the zenith and the azimuth angles (Figure 6). The elevation angle, the complementary of the zenith, is sometimes preferred in other PV simulation software.

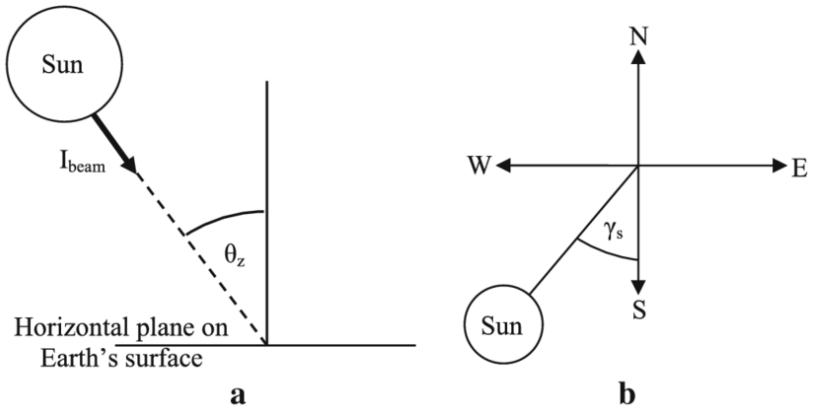

Figure 6. Representation of the sun position: a) Side view showing the zenith (θ_z) b) Top view showing the azimuth (γ_s). Source [34].

Given the sun position at any time, the PV module orientation (module azimuth angle and tilt,

being the latter the module inclination with respect to the horizontal) and the information whether a 1-axis tracking system is enabled or not; the angle of incidence (AOI) between the sun and the PV module can be calculated. This magnitude is of utmost importance for the calculation of the plane of array (POA) irradiance reaching the active PV surfaces. More precise information about the tracking system model, its implication in the module orientation and in the same calculations of the AOI will be commented in chapter 4.2.

As briefly stated in the precedent lines, the AOI takes a special relevance in the calculation of the POA irradiance. The POA irradiance could be divided in its three components: beam, ground-diffuse and sky-diffuse (equation 4.11 in Catalano's thesis). The beam POA irradiance can be directly calculated from the DNI and the AOI (equation 4.12 in Catalano's thesis). Similar to that, the POA ground-diffuse irradiance can be calculated from the GHI, the albedo and the module tilt (equation 4.13 in Catalano's work). Finally, the POA sky-diffuse irradiance can be calculated by means of the Hay-Liu model, shown by Catalano in his equation 4.15.

However, the POA irradiance reaching the solar cells suffers different losses reducing its final value to the so-called "effective POA irradiance":

- **Optical losses** accounted by the incidence angle modifiers (IAM). A different IAM is needed for each irradiance component. Catalano used a methodology for that purpose that is only valid when considering a fixed tilt and tabulated IAM values for the ground-diffuse and the sky-diffuse components. In chapter 4.5.1 of the present work, a revised version of the IAM obtention can be found, with the aim to generalise the methodology to any situation and conditions.
- **Self-shading losses** accounted by factors obtained in the self-shading model. In the case of crystalline silicon technologies (with a non-linear response to shading), only the ground-diffuse and the sky-diffuse components are subjected to the application of these factors, since the effect on the beam component is directly accounted as a DC loss. On the other hand, for thin-film technologies (linear response to shading), the beam component is also subjected to a reduction factor. A brief description of the working principle of the whole self-shading model is provided in the following lines, while a detailed explanation can be found in chapter 4.3.
- **Soiling losses** accounted by an annual average percentage, which can be estimated at a value up to 5% depending on the location [35].

With the previously commented losses, the global effective POA irradiance (after optical, self-shading and soiling losses) can be calculated as follows:

$$E_g = SF \cdot \left(IAM_b \cdot \boldsymbol{SSF_b} \cdot E_b + IAM_{sd} \cdot SSF_{sd} \cdot E_{sd} + IAM_{gd} \cdot SSF_{gd} \cdot E_{gd}\right) \quad (4.1)$$

Where E_g is the global effective POA irradiance; E_b, E_{sd}, E_{gd} are respectively the beam, sky-

diffuse and ground-diffuse POA irradiances; SF is the soiling factor (obtained as the complementary fraction of the soiling losses); IAM_b, IAM_{sd}, IAM_{gd} are the incidence angle modifiers for their respective irradiance components; and SSF_b, SSF_{sd}, SSF_{gd} are the self-shading factors for the beam, sky-diffuse and ground-diffuse components of the irradiance. It is important to notice that SSF_b is highlighted in red, indicating that it is only considered when using thin-film technologies.

The self-shading model, briefly commented before, requires as external inputs the ground coverage ratio (GCR, fraction of area occupied by PV modules to the total area) and the physical layout of the plant (meaning the number of modules along the side and along the bottom of a row; and the total number of modules to compute the number of rows). As results, the self-shading factors to reduce beam (thin-film case), sky-diffuse and ground-diffuse components of the irradiance are obtained (SSF_b, SSF_{sd}, SSF_{gd}), as well as a photovoltaic DC output loss factor (SSF_{DC}) to account for the effect on the beam component when using crystalline silicon technologies. This model is extensively explained in chapter 4.3 and it is based on the model proposed by SAM (System Advisor Model) developers [2].

The IV curve/PV module model computes first the IV curve at reference/standard test conditions with the information coming from the module parameters. Once obtained, the reference IV curve is modified to the particular cell temperature and irradiation conditions at any time, thanks to temperature coefficients for current and voltage (presents in the module parameters) and to the proportional effect on some parameters of the change in irradiance. Then, the maximum power point (MPP) can be computed at any conditions during the whole year and, given the number of modules and its electrical configuration (modules in series per string and number of strings), the power, current and voltages of the array can be obtained. A more detailed explanation of this methodology and of the different sub-models (such as the model to obtain the cell temperature) can be found in section 4.6 of Catalano's Thesis.

The DC output of the PV array is reduced as a consequence of computing differing DC losses. Firstly, DC cabling losses are accounted thanks to a simple model that estimates the equivalent resistance of the DC wirings (section 4.10.1 of Catalano's work). Secondly, several other DC losses are accounted as reduction factors of the resulting DC power. Within this group of losses, the self-shading factor reduction of the DC power (SSF_{DC}) can be included. Other losses factors such as the module mismatch or the diodes connections are also considered. A more detailed and complete explanation of these losses and their computation within the code can be found in chapter 4.5.2 of the present work.

The DC output is transformed to AC thanks to the inverter model. For this purpose, the Sandia inverter model [36] is selected, as commented by Catalano in chapter 4.9 of his work. This model is based on experimental data and is the same one used by SAM. The model needs

the external input of several inverter parameters, which include the operation limits in terms of power, current and voltage as well as the experimental coefficients used by the Sandia model.

This AC output is then reduced as a consequence of computing the AC cabling losses, accounted as a reduction factor of the AC power. Transformer losses are considered out of the scope of the project but can easily be implemented in the same manner as AC cabling losses. A more detailed explanation of these losses can be found in chapter 4.5.3.

Finally, an optional battery model has been implemented during the development of this thesis. The model needs the input of different battery parameters as well as the dispatch strategy or mode of operation. For the sake of the simulation, the mode of operation has been set to providing a flat-output response, a service to the grid of great interest due to reducing the variability of the PV plant output. A detailed explanation of this model and of the dispatch strategy can be found in chapter 4.4.

4.2. Tracking system model

The tracking model implemented corresponds to the so-called 1-axis tracking (or single axis). In this tracking configuration, the rows of PV modules rotate about a horizontal axis orientated north-south, allowing the modules to follow the sun path (from east in the morning to west in the evening). Figure 7 shows the typical configuration of 1-axis tracking PV plants.

Figure 7. 1-axis tracking PV plant. Source: PV Magazine [37].

Figure 7 picture is taken facing the south, thus in this moment PV modules are facing east (modules facing the left part of the picture). The system will follow the sun movement along the day, ending with a west orientation during the evening (modules facing the right part of the picture).

Other tracking systems, such as azimuth axis tracking, 1-axis tracking with tilted rotation axis or 2-axis tracking are out of the scope of this model. Two convergent reasons exist to make

this exclusion decision: none of the omitted tracking systems are seen as cost-effective solutions by experts (suggested by BNEF [38]) and the exclusion of them also simplifies the model formulation.

The proposed model is based on the work of Marion and Dobos in their work *"Rotation Angle for the Optimum Tracking of One-Axis Trackers"* [39]. This is the reference document used by SAM in its tracking implementation. However, the document describes a set of generalised equations allowing tilted 1-axis tracking. For this reason, the present project has simplified these equations to 1-axis horizontal tracking:

$$|\sigma| = abs(\tan^{-1}(\tan Z \cdot \sin(\gamma_s - \gamma_{axis}))) \tag{4.2}$$

Where $|\sigma|$ is the absolute value of the 1-axis tracker rotation angle, Z is the sun zenith, γ_s is the sun azimuth and γ_{axis} is the azimuth angle of the rotation axis. As previously discussed, the tracking device modelled has a rotation axis orientated north-south, that in the sun angles convention taken in the MATLAB code means $\gamma_{axis} = 0°$ (or analogously, $\gamma_{axis} = 180°$).

A convention to decide the sign of the rotation angle σ is taken to define completely the tracking system:

$$\begin{cases} \sigma = 0 & means\ modules\ horizontal \\ \sigma > 0 & means\ modules\ facing\ east \\ \sigma < 0 & means\ modules\ facing\ west \end{cases} \tag{4.3}$$

In order to define the previous convention, the following equation is proposed to calculate the ideal rotation angle:

$$\sigma_{ideal} = -sign(\gamma_s) \cdot |\sigma| \tag{4.4}$$

Equation 4.4 takes the sign of the sun azimuth as an indicator to set the sign for the rotation angle. Since the sun azimuth is negative for east positions and positive for west positions (in our MATLAB notation), a negative sign is added in equation 4.4. This convention is shown in Figure 8.

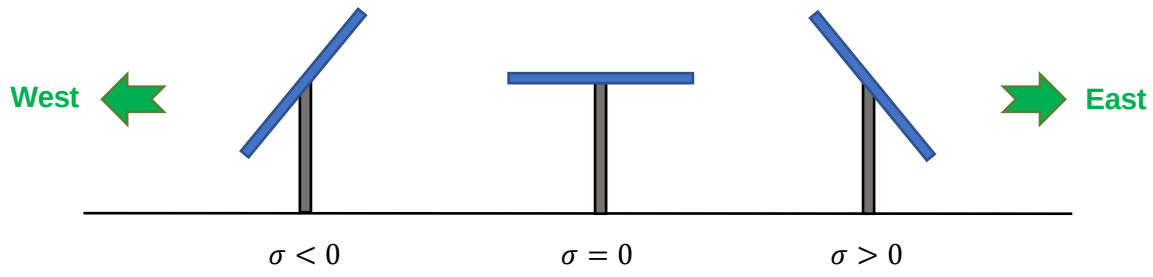

Figure 8. Schematic representation of the 1-axis tracking system and its sign convention for the rotation angle. Source: Own.

Finally, the rotation angle is limited to a maximum angle due to mechanical constraints. A standard rotation limit of ±45º is pre-set, but it is left the user criteria or tracking companies' datasheets. This restriction is implemented into the tracking model as shown in equation 4.5:

$$\begin{cases} -\sigma_{limit} < \sigma_{ideal} < \sigma_{limit}, & \sigma = \sigma_{ideal} \\ \sigma_{ideal} > \sigma_{limit} & \sigma = \sigma_{limit} \\ \sigma_{ideal} < -\sigma_{limit} & \sigma = -\sigma_{limit} \end{cases} \quad (4.5)$$

Once the rotation angle is computed, the tracking model is completed. However, two extra considerations need to be given to include this model to the simulation MATLAB code:

1. When the tracking mode is enabled, the module azimuth is automatically set (and fixed) to face east (-90º in the model convention).
2. Simultaneously, the module tilt is left as a variable that takes the value of the tracking rotation angle at any time.

As it is seen, the previous restrictions are not arbitrary, but a result of the rotation angle convention shown in equation 4.3. Since the azimuth module is fixed to face east, positive module tilts (thus positive rotation angles) will orientate modules to the east. On the other hand, negative module tilts will orientate modules to the west. Note that in simulations with fixed PV arrays (tracking disabled), module azimuth and tilt are two parameters set by the user.

4.3. Self-shading model

The self-shading model proposed in this chapter accounts for the shading losses produced by adjacent rows of PV modules. This kind of loss is relevant and not omissible because of the typical physical layout of PV plants: multiple, parallel and long rows of PV modules. Throughout this chapter, the model presented is based on SAM's self-shading algorithm [2], which in turn is based on the work by Deline et al. (2013) [40].

Before starting the explanation, it is important to remark two options that the model can take:

- **Non-linear option:** refers to crystalline silicon wafer-based technologies. Modules are normally composed by 60 or 72 cells that are grouped in 3 "submodules" determined by the presence of 3 bypass diodes (used to prevent hot-spots). In this case, the response to partial shading is non-linear, since shading in one cell affects all the submodule containing it. To model this non-linearity, the effect on the beam component of the irradiance is accounted as a DC loss factor (SSF_{DC}) explained in chapter 4.3.3.3. The effect on the sky-diffuse and ground-diffuse components is accounted as a reduction factor of the respective irradiance component (chapter 4.3.2).

- **Linear option:** refers to thin-film technologies (CIGS, CdTe and amorphous silicon), which have a linear response to partial shading. This linearity is a consequence of the intrinsic monolithic interconnection of the different cells. The effect on the sky-diffuse and ground-diffuse components is accounted in the same way as in the non-linear option (chapter 4.3.2) while the effect on the beam component is treated also as a linear reduction of irradiance and explained in chapter 4.3.3.2.

The resulting reduction factors (both on irradiance and on DC output) are considered as an average result for the entire array and applied to the complete array. They are calculated for every hour in the year.

4.3.1. Previous calculations of the self-shading model

Some previous calculations related to the plant physical layout are needed before starting the self-shading algorithm.

Firstly, it is important to determine the number of rows of the PV array considered:

$$N_{rows} = floor\left(\frac{N_{modules\_total}}{N_{modules\_side} \cdot N_{modules\_bottom}}\right) \quad (4.6)$$

Where $N_{modules\_total}$ is the total number of modules in the PV array, $N_{modules\_side}$ is the number of modules along the side of each row and $N_{modules\_bottom}$ is the number of modules along the bottom of each row. The concepts of side and bottom of a row can be observed in Figure 9. Equation 4.6 ensures by means of the "floor operator" that the resulting number of rows is an integer. However, for the sake of the calculation accurateness and truthfulness, it is recommended that the user selects the parameters in equation 4.6 in such a manner to ensure an exact integer result.

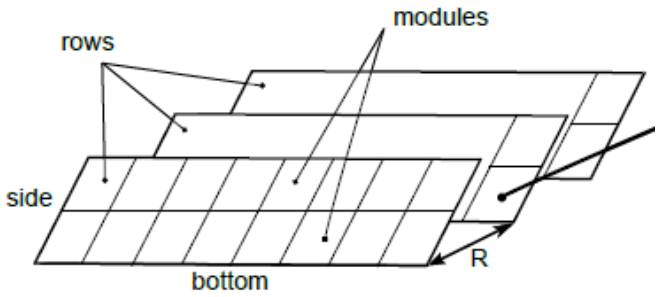

Figure 9. Physical configuration of a PV array with its different rows of modules. Source: SAM [2].

Secondly, it is important to characterise geometrically the PV modules, their length (L) and

width (W). The model takes as inputs the module area (A_m) and the aspect ratio (R_{aspect}), both obtained in the modules' datasheet (Note: the aspect ratio can be easily calculated from the datasheet by dividing module length by module width).

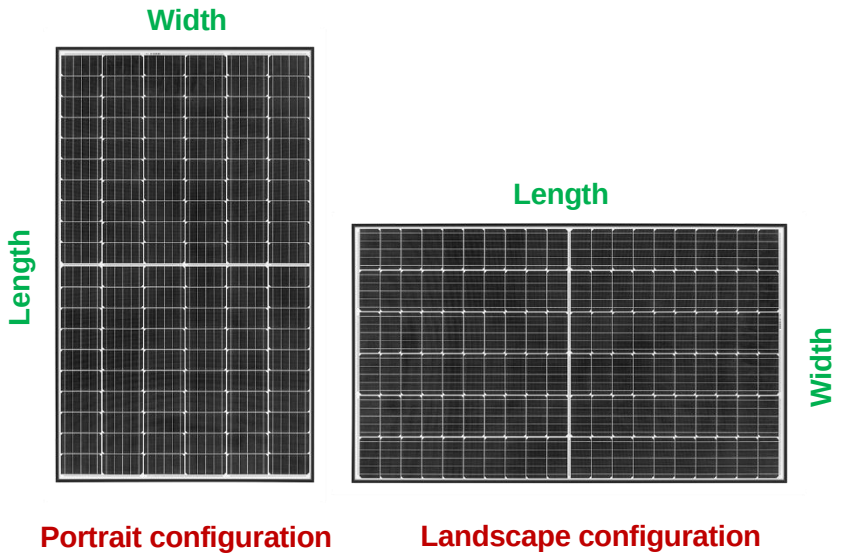

Figure 10. Two possible module configurations: Portrait (left) and landscape (right). Length and width of the modules are also shown. Source: REC Solar [41] + Own.

$$W = \sqrt{\frac{A_m}{R_{aspect}}}$$

$$L = W \cdot R_{aspect} \tag{4.7}$$

Once the geometric characteristics of the modules are known (equations 4.7), the geometric characteristics of the rows (shown in Figure 9) can be calculated: length of the side (L_{side_row}), length of the bottom (L_{bottom_row}) and the spacing between rows (R). It is important to remark that the calculations take different values depending on the module configuration shown in Figure 10.

$$L_{side\_row} = \begin{cases} N_{modules\_side} \cdot L & if\ portrait\ configuration \\ N_{modules\_side} \cdot W & if\ landscape\ configuration \end{cases}$$

$$L_{bottom\_row} = \begin{cases} N_{modules\_bottom} \cdot W & if\ portrait\ configuration \\ N_{modules\_bottom} \cdot L & if\ landscape\ configuration \end{cases}$$

$$R = \frac{L_{side\_row}}{GCR} \tag{4.8}$$

The last line in the group of equations 4.8 calculates the spacing between edges of two adjacent rows by means of the ground coverage ratio (GCR, fraction of area occupied by PV modules to the total area). The GCR for groups of modules arranged in rows can be simplified to the ratio between the side of the row and the spacing between rows. Values of GCR closer to 0 mean low occupancy of land by PV modules while values closer to 1 mean high occupancy.

4.3.2. Effect on the sky-diffuse and ground-diffuse components of the irradiance

The effect of self-shading on the sky-diffuse and ground-diffuse components of the irradiance is the same regardless if the linear option (thin-films) or the non-linear option (crystalline silicon) are used. The resulting factors (SSF_{sd}, SSF_{gd}) are parameters limited between 0 and 1, where values closer to 1 mean no self-shading effect on the studied irradiance component.

4.3.2.1. Effect on the sky-diffuse component

Firstly, the total horizontal diffuse POA irradiance (G_{dh}) is calculated by assuming isotropic sky-diffuse irradiance:

$$G_{dh} = G_d \cdot \left(\frac{2}{1+\cos\beta_s}\right) \tag{4.9}$$

Where G_d is the total diffuse POA irradiance and β_s the module tilt.

Then the shade mask angle (Ψ) must be calculated (equation 4.10). This angle is, according to SAM [2], "the minimum array tilt angle at which the view of the sky at a given point along the side of the row is obstructed by a neighbouring row". A graphical representation of this angle is shown in Figure 11.

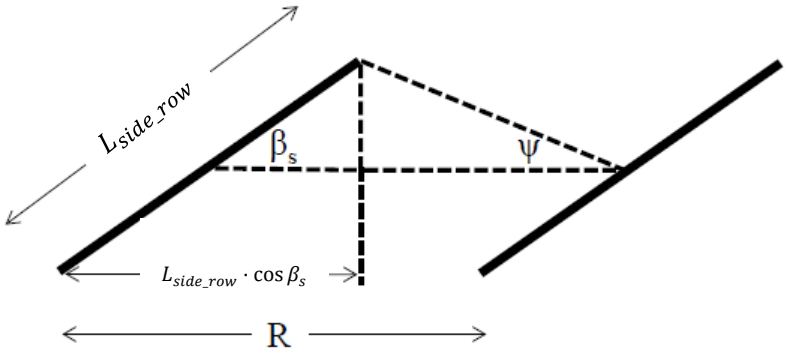

Figure 11. Side view of two adjacent rows showing the mask angle. Source: SAM [2].

$$\Psi = \tan^{-1}\left(\frac{L_{side\_row}\cdot\sin\beta_s}{R-L_{side\_row}\cdot\cos\beta_s}\right) \quad (4.10)$$

In principle, the mask angle should have been calculated by means of an integral all over the module height. However, as suggested by SAM developers, a worst-case scenario strategy can be followed, calculating the shade angle for the bottom of the array.

The reduction in the sky-diffuse POA irradiance can be calculated as:

$$G_{sky\_red} = G_d - G_{dh}\cdot\left(1-cos^2\frac{\Psi}{2}\right)\cdot\frac{N_{rows}-1}{N_{rows}} \quad (4.11)$$

Finally, the sky-diffuse reduction factor is calculated:

$$SSF_{sd} = \frac{G_{sky\_red}}{G_d} \quad (4.12)$$

When the reduction factor in equation 4.12 takes the value of 1, it means that there is no self-shading at all. In addition, when the total diffuse POA irradiance is lower than 0,1 W/m^2, no reduction in the sky-diffuse component is considered.

4.3.2.2. Effect on the ground-diffuse component

Firstly, the beam horizontal irradiance (G_{bh}) must be calculated:

$$G_{bh} = DNI\cdot\cos Z \quad (4.13)$$

It is important to remember that ground-diffuse irradiance is beam irradiance reflected from the ground, thus it is necessary to calculate the length of ground in front of each shaded row that reflects beam irradiance (Y):

$$Y = R - L_{side\_row}\cdot\left(\frac{\sin(180°-\alpha-\beta_s)}{\sin\alpha}\right) \quad (4.14)$$

Where α is the sun elevation (90º - sun zenith).

The view factor of the first row (F_1), the beam reflected component factor (F_2) and the diffuse reflected component factor (F_3) are calculated:

$$F_1 = \rho\cdot sin^2\frac{\beta_s}{2}$$

$$F_2 = \frac{\rho}{2}\cdot\left(1+\frac{Y}{L_{side\_row}}-\sqrt{\frac{Y^2}{{L_{side\_row}}^2}-\frac{2\cdot Y}{L_{side\_row}}\cdot\cos(180°-\beta_s)+1}\right)$$

$$F_3 = \frac{\rho}{2} \cdot \left(1 + \frac{R}{L_{side\_row}} - \sqrt{\frac{R^2}{L_{side\_row}{}^2} - \frac{2 \cdot R}{L_{side\_row}} \cdot \cos(180° - \beta_s) + 1}\right) \quad (4.15)$$

The reduced ground-diffuse irradiance is calculated as follows:

$$G_{ground\_red} = \left(\frac{F_1 + F_2 \cdot (N_{rows} - 1)}{N_{rows}}\right) \cdot G_{bh} + \left(\frac{F_1 + F_3 \cdot (N_{rows} - 1)}{N_{rows}}\right) \cdot G_{dh} \quad (4.16)$$

Finally, the ground-diffuse reduction factor is calculated:

$$SSF_{gd} = \begin{cases} \frac{G_{ground\_red}}{F_1 \cdot (G_{bh} + G_{dh})} & if\ F_1 \cdot (G_{bh} + G_{dh}) > 0 \\ 1 & if\ F_1 \cdot (G_{bh} + G_{dh}) \leq 0 \\ 1 & if\ G_d < 0.1 \frac{W}{m^2} \end{cases} \quad (4.17)$$

4.3.3. Effect on the beam component of the irradiance

Th effect on the beam component is calculated differently depending on the option considered (linear or non-linear) as described at the beginning of this chapter 4.3. The linear option will be explained in chapter 4.3.3.2 while the non-linear option in chapter 4.3.3.3.

Next chapter 4.3.3.1 proposes a set of equations to calculate the shadow dimensions, needed and used by both the linear and the non-linear option.

4.3.3.1. Shadow dimensions

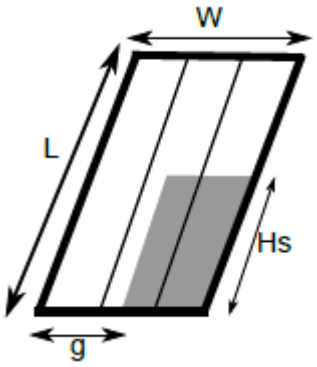

Figure 12. Shadow dimensions defined by the shadow displacement (g) and the shadow height (Hs). Source: SAM [2].

The shadow dimensions are defined by its displacement (*g*) and its height (*Hs*), shown in Figure 12. In addition, it is also possible to observe the 3 submodules in which crystalline silicon modules are divided due to the 3 by-pass diodes that they contain. For the linear case (thin-films) no division in different submodules would appear in its graphical representation.

Before starting the shadow dimensions calculation, a variable change needs to be carried out. This variable modification is a result of the different azimuth notation between the present model and SAM model (the model in which the self-shading algorithm is based on).

Orientation	***Present model***	***SAM model***
North	$\pm 180°$	$0°$
East	$-90°$	$90°$

$\boldsymbol{Orientation}$	$\boldsymbol{Present\ model}$	$\boldsymbol{SAM\ model}$
$South$	0°	180°
$West$	90°	270°

As seen previously, the following change variable needs to be used:

$$\gamma_{SAM} = \gamma_{Present\ Model} + 180° \tag{4.18}$$

Equation 4.18 variable change needs to be applied both for sun and module azimuth angles. From now on, all references to azimuth angles will be considering SAM notation (γ_{SAM}).

Since the original equations proposed by Appelbaum (1979) [42] were intended for always south-facing surfaces in the northern hemisphere, the following modification to the azimuth needs to be considered:

$$\gamma_{eff} = \gamma_s - \gamma_{module} \tag{4.19}$$

Where γ_{eff} is the effective azimuth that is going to be used in this section and γ_s, γ_{module} are the sun and module azimuths respectively.

Next step is the calculation of the shaded portion of the array (divided in the *x* and *y* directions):

$$P_y = L_{side\_row} \cdot \left(\cos\beta_s + \cos\gamma_{eff} \cdot \frac{\sin\beta_s}{\tan(90°-Z)}\right)$$

$$P_x = L_{side\_row} \cdot \sin\beta_s \cdot \left(\frac{\sin\gamma_{eff}}{\tan(90°-Z)}\right) \tag{4.20}$$

Two restrictions need to be added to limit the results of the equation group 4.20. The first restriction nullifies P_y, P_x when $\beta_s = 0$, since no beam self-shading effect can happen when modules are horizontal. The second restriction nullifies P_y, P_x when $\gamma_{eff} > 90°$, since no beam self-shading effect to the adjacent row can happen under this circumstance.

Once the shaded portion is calculated, the shadow displacement can be calculated:

$$g = R \cdot \frac{P_x}{P_y} \tag{4.21}$$

Four restrictions need to be added to equation 4.21:

1. If $g < 0$, then g equals 0, since this means that there is not shadow displacement and all the row is affected by the shadow in the horizontal dimension.
2. If $P_y = 0$, then g equals 0, to avoid infinity and undetermined results.
3. If $N_{modules\_bottom} > N_{modules\_string}$, then g equals 0, since rows are considered to be

extremely long under these circumstances.

4. If $g > L_{bottom\_row}$, then g equals L_{bottom_row}, since the shadow displacement cannot be greater than the length of the bottom of the row.

After the shadow displacement, the shadow height can also be calculated:

$$H_s = L_{side\_row} \cdot \left(1 - \frac{R}{P_y}\right) \tag{4.22}$$

Again, several restrictions need to be imposed:

1. If $H_s < 0$, then H_s equals 0, since this means that the shadow does not reach the module.
2. If $P_y = 0$, then H_s equals 0, to avoid infinity and undetermined results.
3. $g > L_{side\_row}$, then $H_s = L_{side\_row}$, since the shadow height cannot be greater than the length of side of the row.

4.3.3.2. Linear option: reduction of the beam irradiance

For the case of the linear option (thin-films), the following reduction factor for the beam irradiance is calculated:

$$SSF_b = \frac{H_s \cdot (L_{bottom\_row} - g)}{L_{side\_row} \cdot L_{bottom\_row}} \tag{4.23}$$

Equation 4.23 shows the calculation of the reduction factor for the beam irradiance (SSF_b), which is a ratio between the shaded part of the row (numerator) respect to the total row area (denominator). This factor is limited between 0 and 1, where values closer to 1 mean no self-shading effect on the beam component.

4.3.3.3. Non-linear option: self-shading factor reduction of the DC power

For the case of the non-linear option (crystalline silicon), a method to account the effect of the beam irradiance self-shading as a DC power loss factor is explained in this chapter. The method, the one used in SAM software, is based on experimental data.

First, it is necessary to calculate the fraction of each row that is shaded (*X*) and the fraction of submodules shaded in a string (*S*). Different equations are used depending on the module configuration. For the **portrait configuration**:

$$X = ceil\left(\frac{H_s}{L}\right) \cdot \frac{R-1}{R \cdot N_{modules\_side}}$$

$$S = 1 - floor\left(\frac{g \cdot 3}{W}\right) \cdot \frac{1}{3 \cdot N_{modules_{bottom}}} \quad (4.24)$$

And for the **landscape configuration**:

$$X = ceil\left(\frac{H_s}{W}\right) \cdot \frac{R-1}{R \cdot N_{modules\_side}}$$

$$S = \begin{cases} ceil\left(\frac{H_s \cdot 3}{W}\right) \cdot \frac{1}{3} \cdot \left(1 - \frac{floor\left(\frac{g}{L}\right)}{N_{modules_{bottom}}}\right) & if\ H_s \leq W \\ 1 & if\ H_s > W \end{cases} \quad (4.25)$$

In equations 4.24 and 4.25, the number 3 present in both corresponds to the number of by-pass diodes considered (which is the common number of these diodes present in commercial PV modules). Just as a remember, $ceil$ and $floor$ refer to the ceiling and floor operators respectively.

Secondly, the ratio of diffuse irradiance to the total POA irradiance needs to be calculated:

$$R_{diff} = \frac{G_{sky\_red} + G_{ground\_red}}{G_b + G_{sky\_red} + G_{ground\_red}} \quad (4.26)$$

Parameters G_{sky_red} and G_{ground_red} of equation 4.26 have been calculated in chapter 4.3.2, while G_b is the beam POA irradiance.

Moreover, the fill factor is also required for the development of the model, which is calculated from the values at STC of the maximum power, the open-circuit voltage and the short-circuit current:

$$FF = \frac{P_{mpp,STC}}{V_{oc,STC} \cdot I_{sc,STC}} \quad (4.27)$$

With all the above calculated parameters, Deline (2013) [40] proposed the calculation of the following experimental coefficients:

$$C_1 = (109 \cdot FF - 54{,}3) \cdot e^{-4{,}5 \cdot X}$$

$$C_2 = -6 \cdot X^2 + 5 \cdot X + 0{,}28 \quad (but\ if\ X > 0{,}65,\ X = 0{,}65)$$

$$C_3 = max\left[X \cdot \left(-0{,}05 \cdot R_{diff} - 0{,}01\right) + R_{diff} \cdot (0{,}85 \cdot FF - 0{,}7) - 0{,}085 \cdot FF + 0{,}05\ ,\ R_{diff} - 1\right] \quad (4.28)$$

With the three experimental coefficients of equations 4.28, three possible candidates for shade factor can be obtained:

$$F_{shade\_1} = 1 - C_1 \cdot S^2 - C_2 \cdot S$$

$$F_{shade\_2} = \begin{cases} \dfrac{X - S \cdot \left(1 + {}^{0,5 \cdot 3}/_{V_{mpp}}\right)}{X} & if\ X > 0 \\ 0 & if\ X = 0 \end{cases}$$

$$F_{shade\_3} = C_3 \cdot (S - 1) + R_{diff} \tag{4.29}$$

Where V_{mpp} refers to the current maximum power point voltage.

Finally, the self-shading DC power loss factor can be calculated as follows:

$$SSF_{DC} = max\left(F_{shade\_1},\ F_{shade\_2},\ F_{shade\_3}\right) \cdot X + (1 - X) \tag{4.30}$$

The self-shading DC power loss factor is a parameter limited between 0 and 1, where values closer to 1 mean no self-shading effect on the beam component.

4.4. Model of the battery

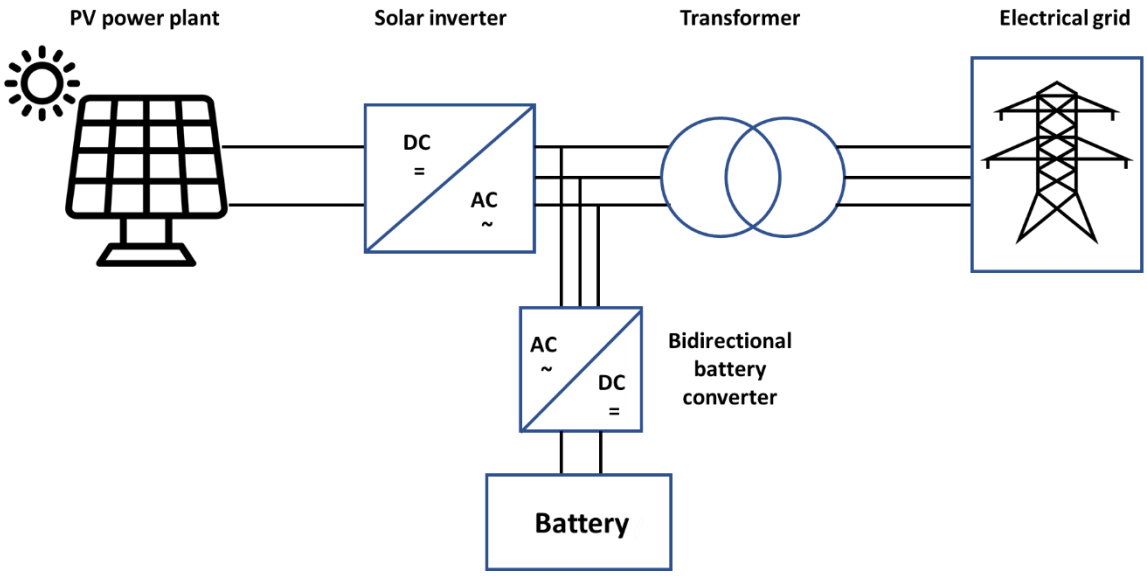

Figure 13. Schematic representation of the PV power plant with the battery connected in the AC side. Source: Own.

The battery model included in this project aims to reproduce a flat-output response for the PV plant [43], which essentially consists in supplying a continuous amount of power the maximum number of hours during a day. This mode of operation could enhance PV plants integration to the electrical grid, since system operators could be able to rely on a more predictable and stable power supply.

Since the goal of the battery model is to provide a first assessment to the flat-output service, a simplified model (Figure 13) with the following assumptions has been chosen:

1. The battery is defined by its energy capacity (Wh or MWh), by its maximum depth of discharge (DOD_{max}, in percentage, the maximum energy extractable from the battery) and by its initial state of charge ($SOC_{initial}$, in percentage) at the beginning of the simulation (January 1st). Moreover, the battery model also includes losses during charging and discharging, represented by their respective efficiencies (η_{charge}, $\eta_{discharge}$).
2. The battery is located in the AC side, since coupling the battery in this part eases the sizing of the solar inverter. In addition, it is realistic to think that existent PV power plants without storage will be retrofitted with batteries in the future, which will be probably AC-coupled.
3. Due to AC-coupling, a bidirectional AC/DC converter is required, which is modelised by a simple converter efficiency ($\eta_{converter}$).
4. The flat-output response is defined as a fraction of the nominal power of the PV plant (*Desired_flat-output_rate*). For example, if the *Desired_flat-output_rate* is set to 60%, the PV plant+storage system will provide (when possible) a 60% of the plant nominal power.

The simplified model does not take into account the instantaneous response profile of a battery. However, since the simulation of the PV plant is done on an hourly basis, a more precise response profile is not required.

Once the assumptions are defined, the battery model algorithm can follow two different situations:

a) PV output > Desired flat-output: in this case, the PV plant output is limited to the desired flat-output and the surplus is stored in the battery (battery charging). If the battery is already 100% charged, the excess energy is lost as heat in the converters or in devices like the DC chopper.

b) PV output < Desired flat-output: the PV plant output is all directed to the grid while the battery provides the lack of energy to reach the desired flat-output (or in case there is not enough energy stored, the maximum energy possible). Note that the battery can never surpass its lower state of charge limit imposed by the maximum depth of discharge (DOD_{max}).

4.5. Other changes and updates of the PV plant model

In this chapter, several modifications to Gabriele Catalano's original code are presented and explained. These modifications are not considered to be completely new models, thus they are explained in this special chapter.

4.5.1. Modification of the incidence angle modifiers (IAM)

In Gabriele Catalano's model for the IAM (present in chapters 4.5.6 and 4.5.7 of his work [1]), a calculation depending on the angle of incidence (AOI) is done for the beam component while tabulated values are used for the sky and ground-diffuse components of the irradiance. This strategy is a good one to avoid calculation time especially when the same module tilt is going to be used. However, if the user decides to vary the module tilt (because of using the tracking model or because of trying to optimise the fixed module tilt), this strategy is no longer valid.

For this reason, this chapter proposes a new calculation for all the IAM, based on the De Soto et al. CEC Module Model (2004) [44]. The new calculation uses the transmittance of the modules to obtain the different IAM.

First, the refraction angle between air and the glass cover of the modules is calculated (remembering that the air refractive index is 1):

$$\theta_{refraction} = \sin^{-1}\left(\frac{sin(\theta)}{n}\right) \tag{4.31}$$

Where θ is the incident angle of light considered (depends on the component of the irradiance studied) and n is the refractive index of glass (1,526 according to De Soto et al.).

Then the transmittance can be calculated as a function of the above-mentioned incidence angle (θ):

$$\tau(\theta) = e^{-KL/\cos(\theta_{refraction})} \cdot \left[1 - \frac{1}{2}\left(\frac{sin^2(\theta_{refraction}-\theta)}{sin^2(\theta_{refraction}+\theta)} + \frac{tan^2(\theta_{refraction}-\theta)}{tan^2(\theta_{refraction}+\theta)}\right)\right] \tag{4.32}$$

Where K is the proportionality constant and L is the thickness of the glass cover (4 m^{-1} and 0,002 m respectively according to De Soto et al.). Angles in equation 4.32 must be entered in radians.

The different IAM can be calculated as a ratio of the transmittances as follows:

$$IAM_b = \frac{\tau(AOI)}{\tau(\theta_{normal})}$$

$$IAM_{sd} = \frac{\tau(\theta_{sd})}{\tau(\theta_{normal})}$$

$$IAM_{gd} = \frac{\tau(\theta_{gd})}{\tau(\theta_{normal})} \quad (4.33)$$

Where IAM_b, IAM_{sd}, IAM_{gd} are the incidence angle modifiers for the beam, sky-diffuse and ground-diffuse components of the irradiance; AOI is the actual angle of incidence between the module and the sun position; θ_{sd}, θ_{gd} are the equivalent incidence angles for the sky-diffuse and ground-diffuse components (to be explained in the following lines) and θ_{normal} is the incidence angle when light incises normal to the module (thus meaning 0º).

As seen, the set of equations 4.33 calculate the different IAM as a ratio between the transmittance at the actual incidence angle to the incidence angle when light incises normal to the module. Theoretically, θ_{normal} should be set to 0º, but to avoid calculation problems, it is set to a very small angle close to 0 (1º to be exact). Finally, the equivalent incidence angles for the sky-diffuse and ground-diffuse are estimated as follows:

$$\theta_{sd} = 59{,}7 - 0{,}1388 \cdot \beta_s + 0{,}001497 \cdot {\beta_s}^2$$

$$\theta_{gd} = 90 - 0{,}5788 \cdot \beta_s + 0{,}002693 \cdot {\beta_s}^2 \quad (4.34)$$

Both equations present in 4.34 are empirical ones and dependent on the module tilt (β_s). In fact, these equations avoid the problem stated by Catalano on the need to perform an integration over all the possible directions the sky-diffuse and the ground-diffuse components can come from.

4.5.2. Inclusion of other DC losses

Following SAM's approach [2], several complicated DC losses to model have been included as DC loss factors. The concerned DC losses are:

- **Module mismatch loss ($L_{mismatch}$):** difference in the performance of the modules connected together induces a DC power loss (modules operate following the lowest performant module). This loss can be accounted to the order of 2% but depends greatly on the converter architecture (using power optimisers nullifies this loss and using string inverter decreases it, while using central inverters maximise it).
- **Diodes and connections loss ($L_{diodes,connections}$):** this loss is caused by voltage drops in the diodes and the connections. SAM estimates it in 0,5%.
- **Tracking loss ($L_{tracking}$):** when tracking is enabled, this loss accounts for the minimal energy consumed by tracker mechanisms.
- **Nameplate loss ($L_{nameplate}$):** this loss refers to a difference between the peak power

at STC announced by the PV module manufacturers and its real value (normally lower). Typical causes for this loss vary from traditional degradation to light-induced degradation (LID, only for the case of p-type mono c-Si) [45].

- **Power optimiser loss ($L_{power\_optimisers}$):** only in the case of using module level power electronics (MLPE) such as power optimiser or micro-inverters, this loss accounts for their effect.

The corresponding DC power loss factors are calculated as follows:

$$F_{DC,i} = 1 - L_i \tag{4.35}$$

Where $F_{DC,i}$ is DC power loss factor for the respective DC loss L_i. Values of DC loss factor close to 1 mean small effect of its respective DC loss.

4.5.3. Inclusion of AC losses

In the present work case, since the transformer is considered out of the scope of the project, only AC wiring losses (L_{AC_wiring}) are accounted. This loss is estimated in 1% and the corresponding AC power factor loss is calculated in a similar way as in equation 4.35.

4.5.4. Update of the weather files

To provide this simulation tool with a broad spectrum of locations to be selected all around the world, an update on the weather files have been carried out. The new weather files have been obtained from SAM's open source database (thus coming from NREL). For the moment, only the files tagged as "*INTL*" (so non-United States locations) can be supported by this simulation tool. A future update of the simulation tool will try to allow the supportability of files tagged as "*SUNY*" (Indian locations) and "*TMY2/TMY3*" (American locations).

4.5.5. Update of the module and the inverter databases

The module and the inverter database have been updated to the most recent version (November 2018) with more than 21000 PV modules and more than 7000 inverters available to be selected. The databases have been obtained from SAM's last version and are originally coming from the California Energy Commission (CEC) as a project included in the initiative "Go Solar California" [46].

4.5.6. Inclusion of the performance ratio (PR) calculation

The performance ratio (PR) is the most adequate quality indicator for PV plants. Since it is a ratio that considers the actual energy produced with respect to the energy produced in ideal conditions (so STC/nominal conditions), its result can provide valuable information for PV

plants owners about real losses of the system. The PR can be calculated as follows [47]:

$$PR = \frac{Y_f}{Y_r} = \frac{{E_{AC}}/{P_0}}{{E_{global}}/{G_{STC}}} \quad (4.36)$$

Where Y_f is the specific yield (kWh/kW$_p$), a measure of the total energy generated per kW$_p$ installed over a certain period of time; Y_r is the reference yield (kWh/kW or peak sun hours), that represents the energy obtainable at ideal conditions with no losses; E_{AC} is the total AC energy output of the PV plant over a period of time (kWh); P_0 is the nominal capacity of the PV plant (kW$_p$); E_{global} is the global POA irradiance reaching the modules (beam + ground-diffuse + sky-diffuse) (kWh/m^2) and G_{STC} is the irradiance at STC (1 kWh/m^2).

Usual values for PR vary between 70-80%, with values reaching 90% considered as really performant PV plants.

4.5.7. Modification of the temperature coefficients

The CEC Module Database includes a coefficient called “adjust” which can be used to modify the voltage and current temperature coefficients given in the same database. This adjust parameter allows to adapt the temperature coefficients given in the manufacturers’ datasheets to a more real value proven by experimental data, according to SAM developers [2]. This modification can be expressed as:

$$\mu_{I_{sc}} = \alpha_{I_{sc,ref}} \cdot \left(1 - \frac{adjust}{100}\right)$$

$$\beta_{V_{oc}} = \beta_{V_{oc,ref}} \cdot \left(1 + \frac{adjust}{100}\right) \quad (4.37)$$

Where $\mu_{I_{sc}}$, $\beta_{V_{oc}}$ are the new calculated temperature coefficients for current and voltage; and $\alpha_{I_{sc,ref}}$, $\beta_{V_{oc,ref}}$ are the temperature coefficients present in the database needed to be corrected. In any case, the inclusion of this modification results in small variations in the final energy output of the plant.

4.5.8. Modification of the sizing model

The sizing methodology presented in the work of Gabriele Catalano (chapter 4.8 of his thesis) has been slightly modified to provide users with more information. Catalano’s work included the sizing of the modules in series, in parallel and of the number of inverters, taking into account the limit operating conditions of the PV array (at minimum or maximum operating temperature or at open-circuit or short-circuit operation, depending on the parameter) and the operating limits of the inverter (current and voltages).

This work also includes the nominal inverter ratio as a sizing parameter. This ratio can be defined as the nominal DC power of the PV array with respect to the nominal AC output of the inverter. Usual values for this parameter vary between 1-1,3, depending on the system characteristics. Values under 1 usually mean under sizing of the system.

PV engineers consider acceptable to have up to 30% more DC nominal power than AC nominal inverter output (Inverter ratio = 1,3) because the DC nominal power is given at STC conditions, which are hardly occurring in a real-life situation. In any case, this parameter serves as a tool to choose inverters and the plant layout which are then refined after simulations.

5. Validation of the new models

The main goal of this section is to validate two of the models added to the MATLAB code: the tracking and the self-shading models.

The validation procedure is simple: a year simulation for a specific location is going to be carried out by SAM (NREL software) and by the MATLAB model used in this work. Both results are going to be compared and assessed so as to validate the models. The location selected to validate the models is Seville (the same one which is used in the case studies).

The third main model added to the code (the battery model) cannot be validated by cross-checking with SAM software. SAM battery model does not allow to simulate the simplified flat-output operation mode used in this work. However, via the battery case study presented in chapter 6.2.4, the proper functioning of this model will be assessed.

5.1. Validation of the tracking model

The tracking model can be validated by cross-checking the tracking rotation angle of the PV modules (defined in chapter 4.2) both in SAM and in the MATLAB code. Figure 14 shows the evolution of the rotation angle during four different days of the year:

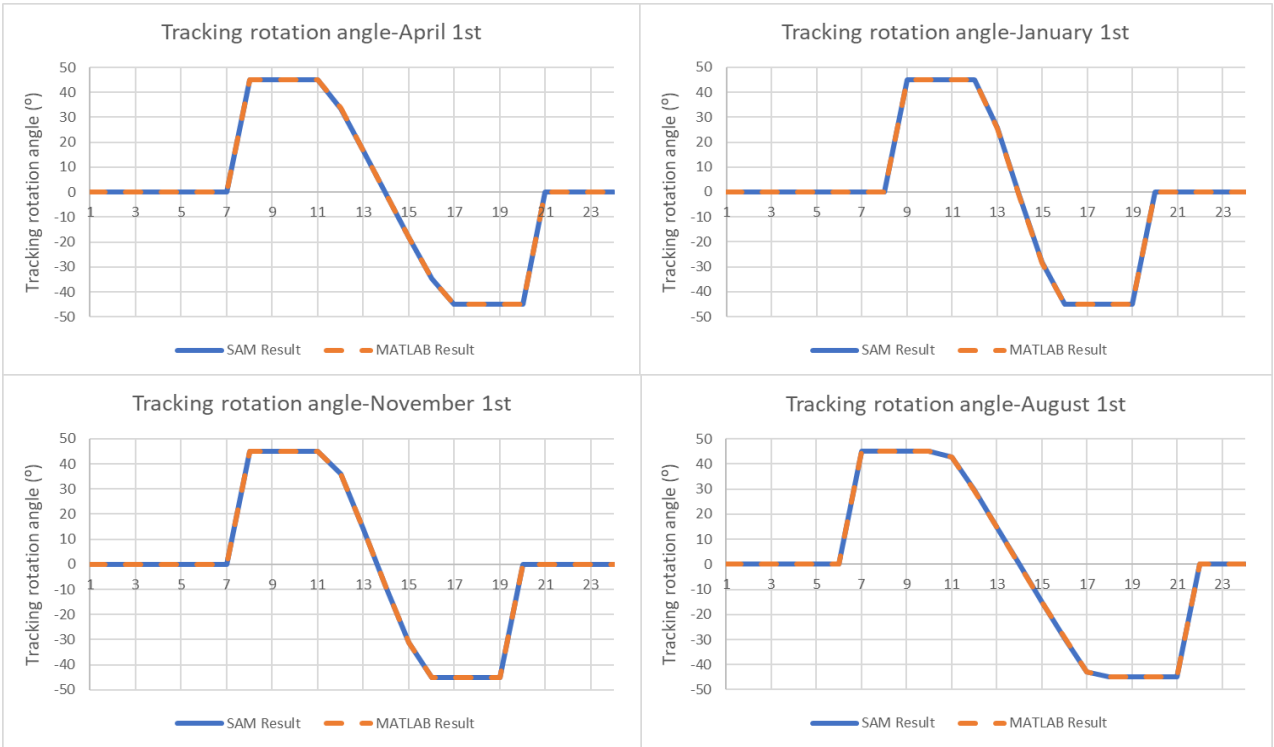

Figure 14. Results comparison for the tracking rotation angle both for SAM and the MATLAB model. Note that the tracking limit has been set to +-45º. Source: Own.

As seen in Figure 14, there are no visible differences between the two simulation results. In this way, the tracking model is confirmed to be valid.

Results for the rest of the year show a similar trend to the one seen in Figure 13. However, for a few days of the year, a slight difference in the sunrise and sunset times between SAM and MATLAB simulations can be observed, inducing a slight delay in the tracking angle at the beginning or at the end of the day. Nevertheless, this difference is not significant in the energy production since it occurs when radiation values are low (early morning and late evening).

5.2. Validation of the self-shading model

Following a similar approach to chapter 5.2, the self-shading model (non-linear option) has been validated in Seville. In order to uniform SAM and MATLAB simulations, the following basic parameters have been set:

- The number of PV modules is 64488. The modules are divided into 5374 strings, each one of 12 modules in series. The goal of this large number of modules is to simulate a considerable number of PV rows.
- Each row is composed by 100 modules, in a configuration of 2 modules in the side and 50 in the bottom of the row (see Figure 9 in chapter 4.3 for more information).
- The PV module used is the *Jinko Solar JKM320PP-72* with an aspect ratio set at 1,7 (this information is only required to know the module size, not for the module performance).
- The ground coverage ratio (GCR) has been set at 80%, a large number to force the maximum self-shading effect possible.

Two yearly simulations have been carried out (one for module portrait configuration and one for landscape), obtaining similar results throughout the year as evidenced by the simulation shown on Figure 15 dated January 1st:

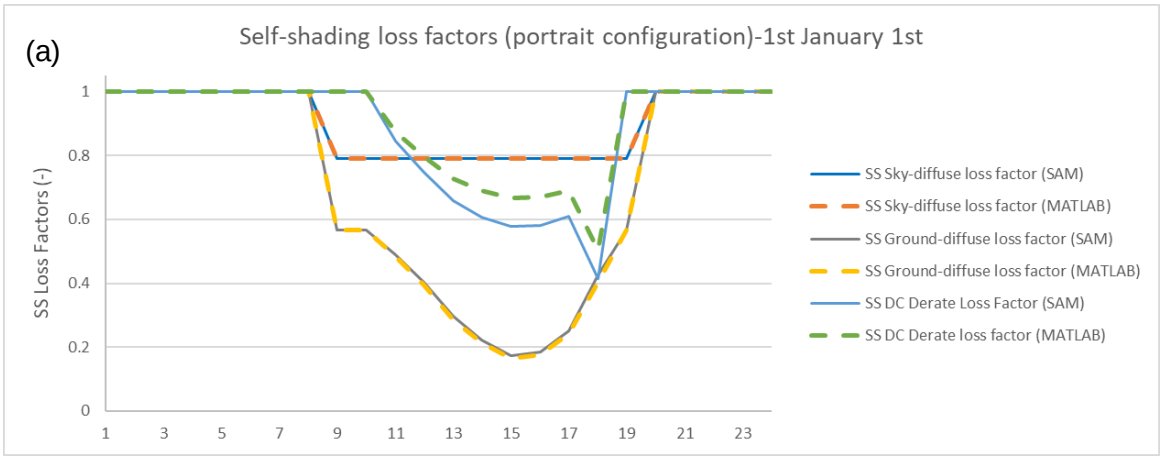

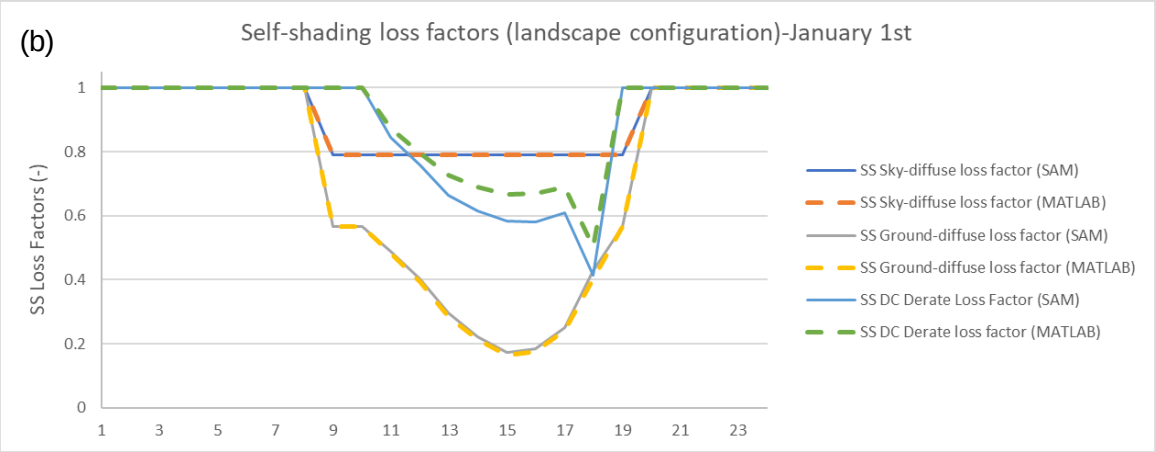

Figure 15. Results comparison between SAM and the MATLAB code for the self-shading (SS) model: portraid (a) and landscape (b) module configurations during the 1st of January. Source: Own

Figure 15 shows the results for the self-shading loss factors both for SAM (solid lines) and for the MATLAB code (dashed lines). As it can be seen, no significant difference can be observed for the ground and sky-diffuse self-shading loss factors. However, for the DC reduction loss factor, the MATLAB model estimates larger factors than SAM (thus lower self-shading effect). The average difference in the DC reduction loss factor is around 1%, meaning that it is consistent between the prediction error of SAM when compared to real PV plants. This allows validating the self-shading model (both for portrait and landscape configurations).

Despite the fact that the above-mentioned difference in DC reduction self-shading estimate is acceptable, several reasons responsible for that are stated in the following lines:

- **Differences in the solar time equations:** SAM equations differ slightly from PVsyst equations (the basis for Gabriele Catalano's original MATLAB code). Moreover, SAM solar time equations allow for weather datasets composed by different years, which is not allowed in the MATLAB code (i.e. SAM weather files can include month data coming from different years to complete a "fictitious" year dataset; and the data year is a parameter included in the solar time equations).
- **Differences between the module size:** the self-shading model proposed in this work uses the module area and the aspect ratio to estimate the module height and width. On the other hand, SAM is allowed to consider the module height and width if available in the database, causing a possible variation with respect to the proposed MATLAB.
- **Differences in the self-shading model restrictions:** equations 4.21 and 4.22 present slight differences in their restrictions when compared to SAM documentation [2], which were considered more appropriate by the author of this work.

6. Case studies: Developing a PV utility-scale power plant in Seville (Spain)

The purpose of this section is to apply the new version of the MATLAB code to the designing and sizing of utility-scale PV plants. For this reason, several case studies are proposed:

- Comparison between string inverter and central inverter architectures. Moreover, different DC/AC ratios will be assessed.
- Inclusion of a 1-axis tracking system.
- Self-shading effect on land-use.
- Inclusion of a battery to provide flat-output.

6.1. General assumptions

6.1.1. PV plant location

The case studies are going to be located in **Seville, Spain**. This location is selected due to its great weather and solar conditions, as well as an increasing favourable environment to PV investment, as explained in chapter 3.4.

6.1.2. PV plant size

The PV plant size considered is **100 MW (DC side)**. This size is of considerable magnitude, but nothing strange in Europe in the coming years, when utility-scale PV sector is going to be further developed.

6.1.3. PV modules

The PV modules selected are manufactured by **JA Solar** (China), one of the top tier cell and module maker [48]. The model selected is the **JAM72S01/PR** [49], a 72-cell monocrystalline PERC module with a peak power of 375 W at STC. Moreover, the module is either compatible with inverter architectures of 1000 V or 1500 V. For fixed-axis simulations, **module tilt** is fixed at **30º**.

6.1.4. Inverters

For the **string architecture**, the market leader in string inverters **Huawei** is selected. The model selected is one of its highest power inverters: **SUN2000-100-KTL-USH0** [50], with 100 kVA of nominal AC power (100 kW of active power if considering cosϕ = 1) and a maximum input voltage of 1500 V.

For the **central inverter**, the well-known German manufacturer **SMA** is chosen. The model selected is one of its highest power central inverters: **Sunny Central-2500-EV** [51], with 2500 kVA of nominal AC power and a maximum input voltage of 1500 V.

6.1.5. LCOE (Levelized Cost of Electricity)

The levelized cost of electricity (€/kWh or €/MWh) can be defined as:

$$LCOE = \frac{I_0 + \sum_{t=1}^{n} \frac{A_t}{(1+i)^t}}{\sum_{t=1}^{n} \frac{M_{t,el}}{(1+i)^t}}$$

LCOE	Levelized cost of electricity in Euro/kWh
I_0	Investment expenditures in Euro
A_t	Annual total costs in Euro in year t
$M_{t,el}$	Produced quantity of electricity in the respective year in kWh
i	Real interest rate in %
n	Economic operational lifetime in years
t	Year of lifetime (1, 2, ...n)

Figure 16. LCOE calculation. Source: Fraunhofer ISE [52].

The equation shown in Figure 16, when applied to PV projects, can be rewritten in the following way:

$$LCOE = \frac{CAPEX + \sum_{t=1}^{n} \frac{OPEX_t}{(1+WACC)^t}}{\sum_{t=1}^{n} \frac{Energy\_to\_grid_t}{(1+WACC)^t}} \quad (6.1)$$

The life expectancy (for LCOE) calculations is of **25 years**.

The **WACC** (Weighted Average Cost of Capital) is the project average return rate to its investors (PV projects are financed by a mix of debt and equity). In the Spanish context, it is estimated at **7%** [53].

The yearly energy injected to the grid ($Energy\_to\_grid_t$) is the output of the MATLAB simulation for the first year. For the subsequent years, a **linear degradation** of the output energy of **0.5% per year** [2] is considered. The degradation of the battery (in case it is included) is also accounted in this factor.

The CAPEX (capital expenditures) is defined by the different components shown in the following table:

CAPEX component	Value	Source
Modules	0,31 EUR/W_p	BNEF [15] and PV experts
String inverters	0,05 EUR/W_{AC}	BNEF [54]
Central inverters	0,03 EUR/W_{AC}	BNEF [54]
BOS (Balance of System)	0,17 EUR/W_p	BNEF [15]
Other costs (EPC, land, etc.)	0,30 EUR/ W_p	BNEF [15]
Tracker cost (if included)	0,05 EUR/W_p	BNEF [38]
Battery cost (if included)	400 EUR/kWh	BNEF [55]

Table 1. PV plant CAPEX divided in its components.

Regarding the OPEX, operational expenditures that are accounted every year of the project lifespan, they can be estimated as follows:

OPEX component	Value	Source
OPEX PV plant	9500 EUR/MW_p	BNEF [56] and PV experts
OPEX tracker	900 EUR/MW_p	BNEF [56] and PV experts

Table 2. PV plant OPEX divided in its components.

6.1.6. PV plant losses

Several PV plant losses are accounted as a percentage of the power output, as explained in chapters 4.5.2 and 4.5.3.

The **module mismatch loss** (caused by the performance differences of modules connected together) is accounted differently depending on the inverter architecture. For **string inverters**, it can be estimated at **1%** of DC output power loss [57]. For **central inverters**, it is estimated slightly higher at **1,25%** [57]. This difference is due to the different position of the MPPT (Maximum Power Point Tracker) which is included within the inverter: the more modules are controlled together by the same MPPT, the higher is the module mismatch loss. Remember that using power optimisers or microinverters at module level would nullify this loss.

The **diodes and connections loss** is estimated at **0,5%** of the DC output as suggested by

SAM [2].

The **tracking loss** (when the tracking model is enabled) is estimated at **0,1%** of the DC output, since only takes into account the tracker self-consumption.

The **nameplate loss** is estimated at **1%** of the DC output [58] and accounts for the typical p-type monocrystalline modules power reduction in the first months due to LID (Light-Induced Degradation).

The **power optimiser loss** is set at **0%** of the DC output, since no power optimisers are used in this project (not yet a cost-effective solution for utility-scale, though a great solution for the residential sector).

The **AC wiring loss** is estimated at **1%** of the AC output [2].

6.1.7. PV plant layout

The following table summarises the plant layout for the different configurations used in the case studies:

	String inverter architecture	Central inverter architecture
Modules per string (series)	26	28
Total number of strings	10.250	9.518
Total number of modules	266.500	266.504
DC nominal power (kW_p)	99.937,5 kW_p	99.939 kW_p

Table 3. PV plant layout depending on the inverter architecture selected.

The plant layouts shown in Table 3 have been obtained by sizing the system together with the corresponding inverter, thus meaning respecting the current and voltage constraints stated in the datasheets.

The number of inverters to use varies depending on the DC/AC inverter ratio considered in the case studies. For example, for a DC/AC ratio of 1, **1000 string Huawei inverters** are required while only **42 central SMA inverters** are needed. Since several DC/AC ratios are going to be studied, the number of inverters and strings per inverter (or per array) are going to be further discussed during the next chapter.

6.2. Case studies development

6.2.1. String vs central inverter architecture under different DC/AC inverter ratios

This first case study has the objective to deal with one of the hottest topics in the PV industry: the choice between string inverters or central inverters, which is basically a fight between distributed or centralised architectures of PV plants.

String inverters allow for a better control of the plant performance, since the inverter MPPTs control a lower amount of PV modules, reducing in this way the module mismatch loss. Moreover, string inverters also allow for a better reliability of the output power, since a failure in one of the inverters only disconnects a small fraction of the PV plant. On the negative side, as seen in Table 1, the CAPEX of the PV plant is increased as a consequence of a larger number of inverters required to be installed.

Figure 17. Typical image of a PV plant with string inverters (NOTE: The string inverters seen in this figure are of lower nominal power than the used in this work). Source: Huawei [50].

On the other hand, central inverters benefit from a significant cost advantage due to economies of scale (here understood as more AC power output packed in one device/inverter) and lower installation complexity. However, a larger amount of PV modules is controlled by the same inverter MPPTs, increasing module mismatch losses; and reliability is seriously compromised

when a single inverter fails.

Figure 18. Typical image of a PV plant with central inverters. Source: SMA [51].

6.2.1.1. Specific layout of the different configurations proposed

In this case study, three different configurations per each inverter type are proposed, thus meaning a total of 6 configurations studied (3 string inverter configurations and 3 central inverter configurations).

Since the goal is to compare and assess differences between string and central inverter but on the same basis, DC/AC inverter ratios must serve as the common ground for the comparison (taking into account that the nominal DC power is already fixed at 100 MW). Bearing that in mind, the following configurations are proposed:

	Configuration string 1	**Configuration central 1**
Inverter type	String	Central
AC/DC inverter ratio	≈ 1	≈ 1
Total Number of inverters	1000	42
Modules per string (series)	26	28

Strings per inverter (approx.)[1]	10 to 11	226 to 227
Total number of strings	10.250	9.518
Total number of modules	266.500	266.504
DC nominal power (kW_p)	99.937,5 kW_p	99.939 kW_p
AC nominal power (kW_{AC})	100.000 kW_{AC}	98.862,54 kW_{AC}

Table 4. PV plant configurations for a DC/AC inverter ratio of 1.

	Configuration string 2	**Configuration central 2**
Inverter type	String	Central
AC/DC inverter ratio	≈ 1,15	≈ 1,15
Total Number of inverters	870	37
Modules per string (series)	26	28
Strings per inverter (approx.)[1]	11 to 12	257 to 258
Total number of strings	10.250	9.518
Total number of modules	266.500	266.504
DC nominal power (kW_p)	99.937,5 kW_p	99.939 kW_p
AC nominal power (kW_{AC})	87.000 kW_{AC}	87.093,19 kW_{AC}

Table 5. PV plant configurations for a DC/AC inverter ratio of 1,15.

[1] The number of strings per inverter could vary depending on the considered array (e.g. 10 to 11 means that the inverters in this configuration have either 10 or 11 strings connected to them). This comes as a result of imposing a total nominal PV plant output, but does not imply technical feasibility problems.

	Configuration string 3	Configuration central 3
Inverter type	String	Central
AC/DC inverter ratio	≈ 1,3	≈ 1,3
Total Number of inverters	769	33
Modules per string (series)	26	28
Strings per inverter (approx.)[1]	13 to 14	288 to 289
Total number of strings	10.250	9.518
Total number of modules	266.500	266.504
DC nominal power (kW_p)	99.937,5 kW_p	99.939 kW_p
AC nominal power (kW_{AC})	76.900 kW_{AC}	77.677,71 kW_{AC}

Table 6. PV plant configurations for a DC/AC inverter ratio of 1,3.

Tables 4, 5 and 6 show the different configurations studied depending on the inverter ratio (1, 1,15 and 1,3 respectively). It is interesting to note the *AC nominal power* row in each table: while in string configuration cases the AC nominal power matches as a multiple of its inverter nominal power (100 kW, chapter 6.1.4), the central inverter cases don't. This is a consequence of a divergence between the inverter nominal power stated by the manufacturer (2500 kW) and the CEC Inverter Database (2353,87 kW). This project has decided to follow the CEC Inverter Database, the one used in the calculations.

6.2.1.2. Results

Table 7 summarises the results obtained for the different PV plant configurations:

	String 1	Central 1	String 2	Central 2	String 3	Central 3
CF (%)	22,83%	22,47%	22,83%	22,46%	22,59%	22,32%
Inverter losses (%)	1,57%	2,87%	1,57%	2,95%	2,60%	3,53%
Clipping losses (%)	0%	0%	0,006%	≈ 0%	1,02%	0,48%
PR (-)	0,8491	0,8357	0,8491	0,8351	0,8402	0,83
LCOE (EUR/MWh)	49,3910	49,0987	49,0525	**48,9477**	49,3009	49,0921
Energy Y1 (MWh)	170.574,9	167.882,4	170.565,4	167.754,4	168.788,4	166.745,7

Table 7. Summary of the results obtained by the different PV plant configurations (CF-Capacity Factor, PR-Performance Ratio, LCOE-Levelized Cost of Electricity, Energy Y1-Energy during year 1).

As seen in Table 7, string inverter configurations tend to perform better (higher *PR*) and produce more energy than their homologous central inverter configurations. However, when considering *LCOE*, central inverters position themselves as the most cost-effective solutions. These results confirm the working principle of both inverters: string inverters reduce module mismatch losses but at a higher cost than central inverters. In addition, since the power rating in central inverters is higher, inverter losses also tend to be higher. (NOTE: Inverter losses accounts for all the inverter power loss, including efficiency and clipping among others. However, due to the relevance of clipping losses, they are also presented in the results table).

The best solution of this case study is **Configuration central 2**, which has the lowest *LCOE* among all the solutions: 48,9477 EUR/MWh (or 0,0489 EUR/kWh). This value is in accord with recent PV projects developed in South Europe and confirms the Spanish PV sector as a competitive source of electricity.

Configuration central 2 has a DC/AC inverter ratio of 1,15, confirming that under-sizing the inverter (having a higher DC capacity -modules capacity- than AC capacity -inverters capacity)

can contribute to obtain cost-effective solutions. However, the previous statement has a limitation: clipping losses. Clipping losses occur when the PV plant DC output is higher than the maximum DC input power allowed by the inverter (and the inverter *clips out*). This situation normally occurs few times (or never) if the plant is well sized, especially in sunny days. Thus, clipping losses are accepted if the overall solution shows to be cost-effective (note that *Configuration central 2* has a "≈" symbol in Table 7 due to the presence of residual clipping losses). A graphical visualisation of the clipping losses effect can be seen in Figure 19, where the DC and AC PV production is plotted for July 19th in *Configuration Central 3* (the day with the highest clipping losses in the worst PV plant configuration, from a clipping point of view):

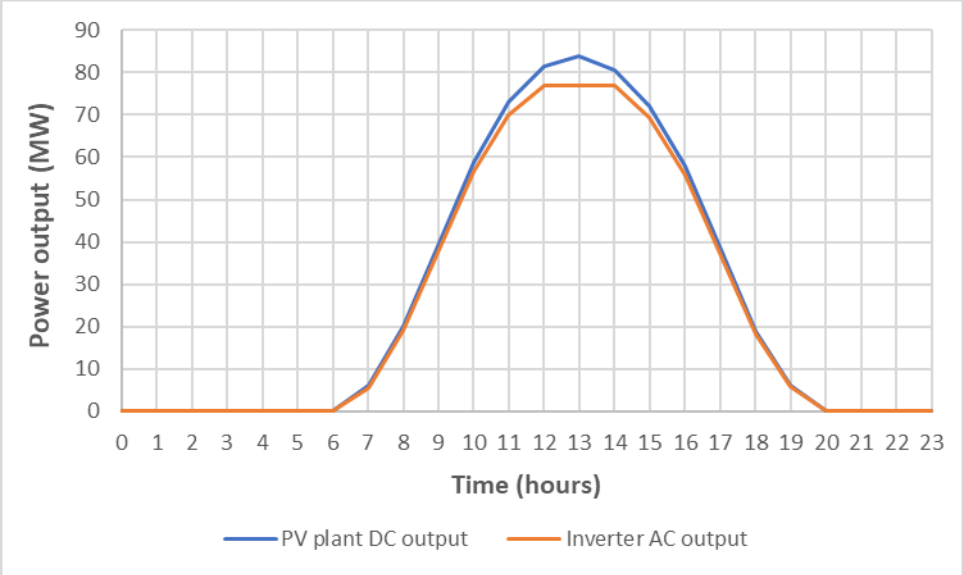

Figure 19. DC (blue line) and AC (orange line) output of the PV plant (configuration central 3) for July 19th, evidencing the occurrence of clipping losses.

As seen in Figure 19, the inverter AC output follows the PV modules DC output (minus losses) until 12 pm, when the inverter clips out and the AC power output is limited to the nominal capacity of the inverters (77,7 MW minus AC wiring losses) until 14h (2 pm). It is also interesting to see that, in one of the days with higher PV production, the DC output falls way apart of the plant peak power of 100 MW. The plant peak power is defined at STC (Standard Test Conditions): 1000 W/m^2, 25 ºC and AM (air mass) 1,5; ideal conditions difficult to attain in real projects.

6.2.2. Inclusion of a 1-axis tracking system

The inclusion of tracking devises is another of the hottest topics among PV project developers, and the focus of this second case study. More exactly, 1-axis tracking systems that follows the sun from east to west (chapter 4.2 for an exact definition) are studied.

1-axis tracking are expected to become mainstream during the next decade, as stated by the German PV manufacturers association (VDMA-PV) in its annual ITRPV report (International Technology Roadmap for Photovoltaic) [20]: 1-axis tracking system will increase their share in utility-scale PV from around 20% in 2018 to over 50% in 2029.

The reasons for this impressive share growth are rooted to the cost-effectiveness of the solution: by increasing slightly the system CAPEX and OPEX (Tables 1 and 2), the PV modules can generate more electricity by following the sun throughout the day. Especially advantageous is the possibility to start producing electricity earlier in the morning and finishing the production later in the evening, allowing more production hours and a flatter PV plant output.

Regarding the 1-axis tracker cost present in Table 1 (0,05 €/W_p), it is important to comment that this value represents the add on the total system CAPEX. In reality, tracker cost is around 0,10 €/W_p, but this also accounts for the mounting structures. Mounting structures for fixed-axis systems can be estimated at 0,05 €/W_p, thus the real tracker cost add on total CAPEX needs to subtract the savings in these mounting structures [38].

The considered best configuration of the previous case study (**configuration central 2**) will serve as the baseline for the inclusion of a 1-axis tracking system. Moreover, the tracker angle of rotation is limited to ±45º, due to mechanical constraints.

6.2.2.1. Results

The following Table 8 shows a comparison between the PV plant (in *configuration central 2*) with and without the inclusion of a 1-axis tracking system:

	No trackers (fixed axis)	1-axis trackers
CF (%)	22,46%	24,78%
Inverter losses (%)	2,95%	2,88%
Clipping losses (%)	≈ 0%	0%
PR (-)	0,8351	0,8388
LCOE (EUR/MWh)	48,9477	**47,2850**
Energy Y1 (MWh)	167.754,4	185.109,8

Table 8. Summary of the results obtained by the PV plant configuration central 2 with and without tracking system (CF-Capacity Factor, PR-Performance Ratio, LCOE-Levelized Cost of Electricity, Energy Y1-Energy during year 1).

As seen in Table 8, the superior energy production of the plant with 1-axis trackers (more than 10% increase in energy production) allows to compensate for the extra investment in CAPEX (explained in chapter 6.1.5). The result is a superior cost-effectiveness of the PV plant with trackers (more than 3% decrease in LCOE).

In addition, depending on the location and by being more optimistic in the assumptions of tracker system cost and rotation angle limits, notable publications state that a 10% reduction in LCOE could be attainable [38]. Therefore, trackers are considered a very interesting solution for improving PV plants performance (as long as enough land is available to deal satisfactorily with self-shading).

Coming back to the Spanish context, one of the top tracker suppliers, *Soltec* (5th world supplier in 2018, according to *IHS Markit*) is a Spanish based company, enhancing local knowledge of these solutions.

Another interesting feature to observe is the comparison on a monthly basis (Figure 20):

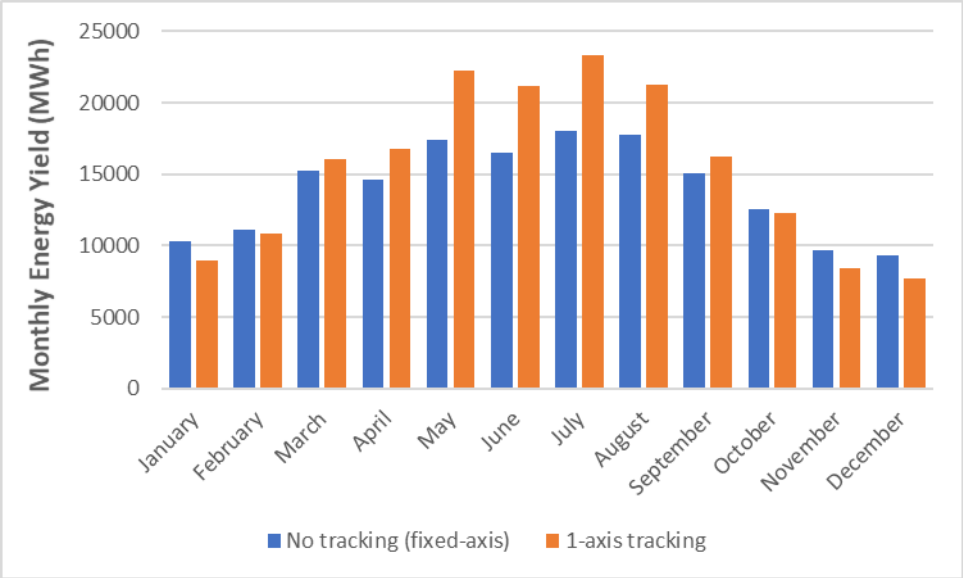

Figure 20. Monthly energy yields for the PV plant with no tracking (blue) and with tracking (orange).

As seen in Figure 20, the tracking option has a superior energy yield during the summer months (when the sun is higher in the sky). However, during the winter months, the tracking solution has no advantage at all (even it can produce slightly lower). A lower winter sun altitude induces a better angle of incidence for fixed-axis modules tilted and facing the south, translating into a slightly higher energy production. Notwithstanding, the higher production during summer months allow 1-axis tracking plants to overproduce fixed-axis plants at the end of the year. Note that this reasoning is valid for the northern hemisphere, but a plant in the southern hemisphere would have a similar reasoning (inversed from summer and winter months perspective).

Finally, it is also interesting to observe the comparison in solar production during some selected day: the summer and the winter solstices (June 21st and December 21st) when the sun altitude is the highest and the lowest respectively (in the northern hemisphere):

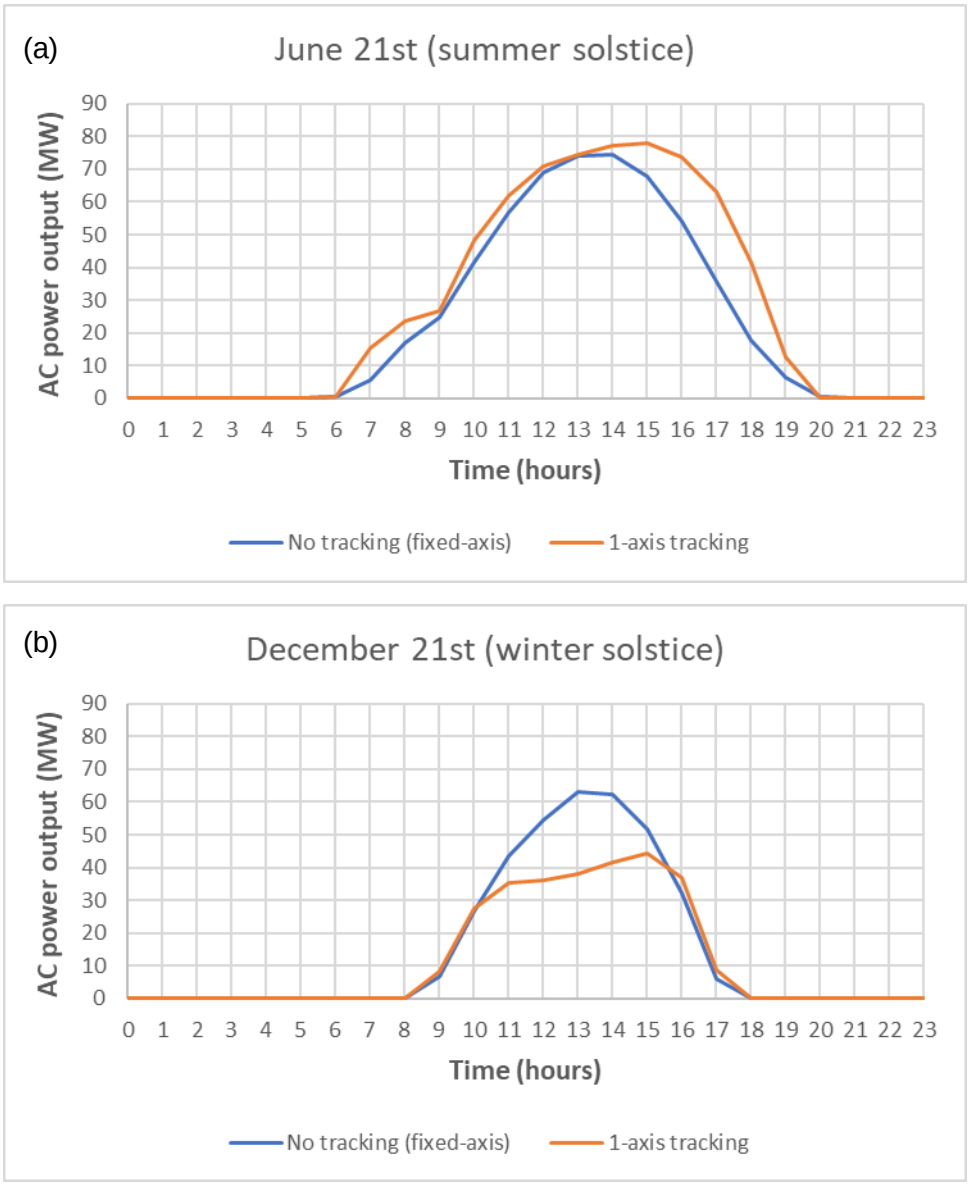

Figure 21. Comparison between the daily AC output of the PV plant with no tracking (blue) and with tracking (orange): a) June 21st b) December 21st.

As seen in Figure 21-a, during summer days, the 1-axis tracking PV plant starts producing electricity earlier in the morning and ends production later in the evening. This fact is relevant, since the PV plant will be able to help the national power system to ramp up production to prepare for the night consumption peak.

However, during the winter solstice (Figure 21-b), it can be observed that production with a tracking system is lower due to a worst angle of incidence (discussed in the previous page). Fortunately, this only happens few days during the year, concentrated at the end of November, December and beginning of January, when solar potential is lower in Spain and in Europe.

6.2.3. Self-shading effect on land-use

Typically, PV power plants consist of multiple parallel rows of PV modules. Between them, a certain space is left void to ensure a minimum effect of shading between rows (the so-called self-shading). However, taking into account that land availability is a finite magnitude, it is important to find a compromise between self-shading losses and land use. This topic takes a special relevance in Europe, where the development of utility-scale solar is strongly related to land availability constraints. Other regions with large extensions of non-populated land, such as deserts in the Middle East or Northern Africa, are not as exposed to this treat as in the European case. This is the reason why a self-shading model was considered a key element to include in the MATLAB simulation code, and its assessment is the focus of this case study.

Again, the considered best inverter configuration in chapter 6.2.1.1 will be the baseline for this case study (**configuration central 2**). PV plants with tracking systems are out of the scope of the present self-shading model, as commented in chapter 2.2. The following Table 9 shows the general assumptions of the self-shading model (both for portrait and landscape module configurations), with Figure 22 being a recall of the model nomenclature:

	Portrait configuration	**Landscape configuration**
Modules in the side of each row	2	4
Modules in the bottom of each row	250	125
Total number of modules per row	500	500
Total number of rows in the PV plant	533	533
PV module aspect ratio (height to width)	1,7	1,7

Table 9. General assumptions of the self-shading model

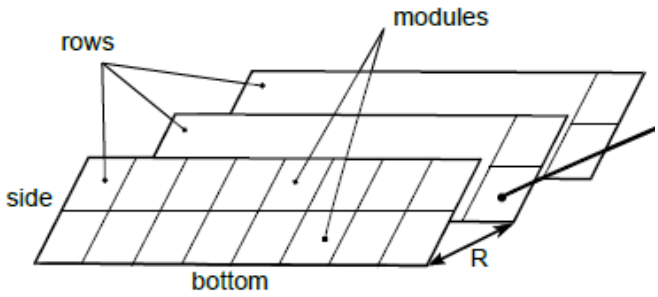

Figure 22. Physical configuration of a PV array with its different rows of modules. Source: SAM [2].

The fact of having a different row layout for portrait and landscape configurations is an attempt to make them comparable from a self-shading point of view: it just does not make sense to compare each configuration with the same number of modules in the side of the row, since the portrait case will always produce much more shadows (length of a module is greater than its width).

An extra parameter is left free to generate the different cases studied: the ground coverage ratio (GCR, fraction of area occupied by PV modules to the total area). Two different GCR are going to be tested for both module configurations:

- GCR = 0,3: meaning a space between rows of 12 m (portrait configuration) and 14 m (landscape configuration).
- GCR = 0,6: meaning a space between rows of 6 m (portrait configuration) and 7 m (landscape configuration).

Note that the inter-row spacing is indicated as *R* in Figure 22.

The proposed cases studied in this chapter are only a few of the infinite possible row layouts. In real PV projects, the inter-row spacing, the row layout and the module configuration are often decided depending on the location specific characteristics.

6.2.3.1. Results

Table 10 summarises the key indicators of the PV plant for the self-shading case studies (always considering *Configuration central 2* as the base case study):

	Portrait GCR=0,3	**Portrait GCR=0,6**	**Landscape GCR=0,3**	**Landscape GCR=0,6**
CF (%)	22,32%	20,81%	22,32%	21,26%
Inverter losses (%)	2,95%	2,95%	2,95%	2,95%
Clipping losses (%)	0%	0%	0%	0%
PR (-)	0,83	0,7738	0,83	0,7906
LCOE (EUR/MWh)	49,2439	52,8196	49,2385	51,6972
Energy Y1 (MWh)	166.745,4	155.457,3	166.763,5	158.832,3

Table 10. Summary of the results obtained by the PV plant configuration central 2 with the self-shading model enabled (CF-Capacity Factor, PR-Performance Ratio, LCOE-Levelized Cost of Electricity, Energy Y1-Energy during year 1).

Table 10 shows the results obtained when enabling the self-shading model for the different module and GCR configurations.

As it can be seen, a GCR of 0,3 (i.e. 30% of the land occupied by PV modules) has a low effect on the plant performance both for portrait and landscape configuration (*PR* is decreased by a merely 0,5% and *LCOE* is worsened by 0,6% roughly). In fact, a 30% occupancy of land is a popular value between developers of large-scale PV plants if space is available, since self-shading effect is almost neglectable.

However, when GCR is increased to 60%, annual energy production is reduced by around 6% for portrait configuration and 5% for landscape due to self-shading losses. This lower energy production impacts increasing *LCOE* for both cases - between 2 and 3 EUR/MWh. It is interesting to observe the impact of the self-shading losses on POA irradiance and DC output (Table 11). As a quick recall of chapter 4.3, since the case study considers the non-linear option, self-shading loss factors affect ground and sky-diffuse components directly on the POA irradiance while beam component is affected on the DC output.

	Portrait GCR=0,6	**Landscape GCR=0,6**
Self-shading loss on irradiance (%)	3,33%	3,33%
Self-shading loss on DC output (%)	4,43%	2,36%

Table 11. Self-shading losses impact (in percentage) on diffuse (loss on irradiance) and beam (loss on DC output) components for portrait and landscape configurations.

As seen in Table 11, self-shading impact on diffuse components (ground and sky) is almost the same independently of the module configuration (portrait or landscape). In fact, equations of the self-shading model for these components of the irradiance (chapter 4.3.2) confirm the small dependence on module configuration.

On the other hand, self-shading impact on DC output (and thus on the beam component) is completely dependent on the module configuration. The answer can be found in the non-linear response of c-Si modules to shading. More precisely, c-Si cells are connected in series to form modules, with three bypass diodes serving as protection against hotspots. Each bypass diode protects 1/3 of the module cells, creating “3 submodules”. If only one of these cells is shaded and performs below the rate of rest, the complete group of cells in the submodule is disconnected by the diode. As suggested in the beginning of this paragraph, the module configuration has a great impact on the final output. Let’s imagine a worst-case scenario where a shade strip appears in the lower part of the modules (Figure 23):

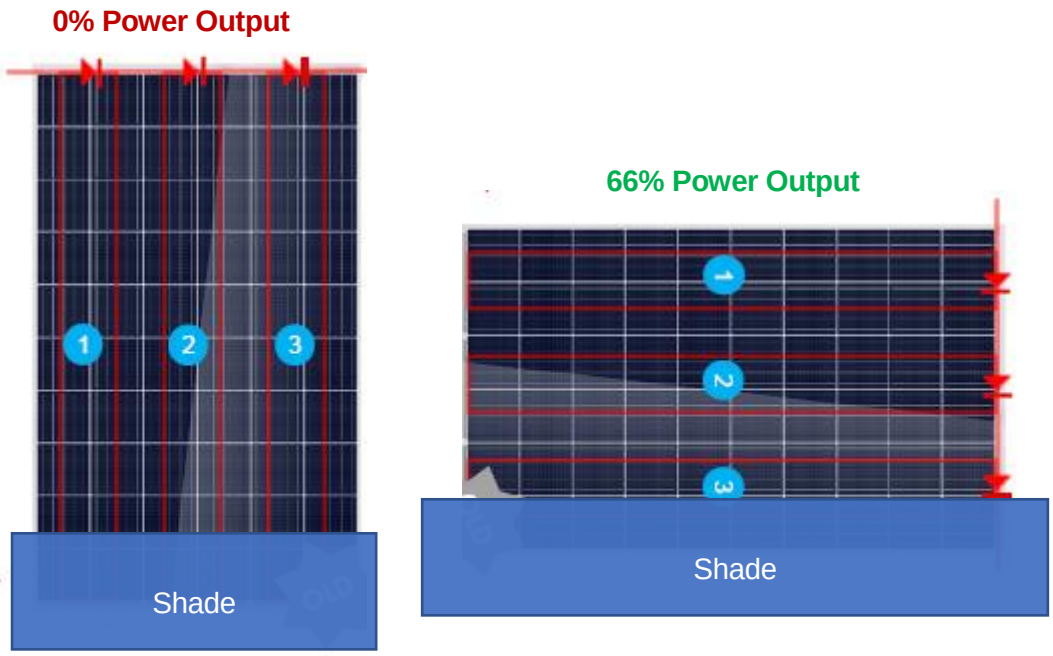

Figure 23. Illustration of the power output under shading for portrait (left) and landscape (right) module configurations. Note that the shade strip produces total shading of the affected cells. Source: Trina Solar + Own.

In portrait configuration (left in Figure 23), the shade strip affects cells in the lower part of the module, forcing all bypass diodes to enter conduction mode (setting power output to 0).

On the other hand, in landscape configuration (right in Figure 23), a similar shade only forces one bypass diode to enter conduction mode, losing 33% of the module rated power (66% of power output still remains).

Coming back to the present case study, row-to-row self-shading produces similar effects to the ones shown in Figure 23, reason why landscape configuration has a better performance.

Finally, concerning land use, a dilemma appears: **reducing self-shading losses increases land use and vice versa**. The 100 MW plant will occupy around 0,5 km^2 in PV modules (same value for both module configurations). Considering the different ground coverage ratios:

- If **GCR=0,3**, the PV plant land requirements will be of **1,67 km^2**.
- If **GCR=0,6**, the PV plant land requirements will be of **0,84 km^2**.

Figure 24 shows the evolution of self-shading DC output losses (the most important self-shading effect) against land use:

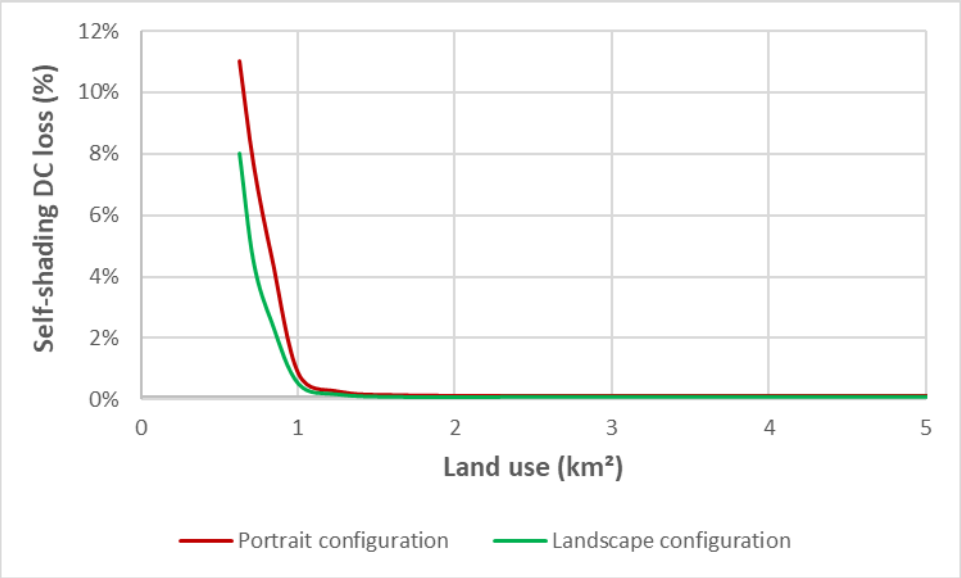

Figure 24. Self-shading DC los against land use for portrait (red) and landscape configuration.

As it can be seen, Figure 24 evidences the statements discussed in the previous page: the lower the land use, the more losses due to self-shading. Interestingly, the non-linear shading effect of c-Si modules is clearly appreciated, as well as the higher vulnerability of portrait modules to self-shading.

Again, as in the other case studies, there is not a unique choice for module configuration and row-to-row spacing. It largely depends on the location characteristics and even on the project developer preferences. In our case, the **selected PV plant** will be the **landscape configuration with GCR=0,3**, since self-shading losses are almost neglectable and land use is acceptable.

6.2.4. Inclusion of a battery to provide flat-output

Finally, the last case study is focused on the inclusion of a lithium-ion battery to provide a flat-output response the maximum hours per day. This case study is also of important relevance when considering that the world's power systems are increasing the capacity share of intermittent and difficult to predict renewable energies (such as solar PV). Thus, providing a more predictable output with a simple battery discharge strategy could play a very important role in future power systems.

Again, the considered best inverter configuration in chapter 6.2.1.1 will be the baseline for this case study (**configuration central 2**). But in this case, to perform a more real simulation, the self-shading model with **landscape configuration and GCR=0,3** is activated.

The general assumptions of the battery are the following ones (see chapter 4.4 for more information about the parameters):

Battery capacity (MWh)	125 MWh [2]
$SOC_{initial}$ (January 1st) (%)	50%
DOD_{max} (%)	90%
Bidirectional converter efficiency (%)	98%
Battery charge efficiency (%)	98%
Battery discharge efficiency (%)	98%

Table 12. General assumptions for the battery model, with typical efficiency values.

With the general parameters of the battery defined (Table 12), two cases are proposed to study, depending on the flat-output rate desired:

- *Desired_flat-output_rate = 50% of the PV plant nominal capacity*, thus meaning a desired flat-output AC power (injected to the grid) of around 50 MW.
- *Desired_flat-output_rate = 70% of the PV nominal capacity*, thus meaning a desired flat-output AC power (injected to the grid) of around 70 MW.

The above stated desired flat-outputs rates set the power to be injected to the grid the maximum number of hours possible (just until the battery runs out of energy).

The battery system cost shown in Table 1 (400 €/kWh) includes, among others: the battery pack, the battery BOS, the energy management system (EMS), the power conversion systems (PCS, bidirectional converter), the EPC cost, developer overheads or developer margin [55].

Since main goal of this study is to understand and assess the flat-output response performance; a 1-year MATLAB simulation will be enough. However, to assess the economic impact of this option, LCOE calculation is required. This project assumes that battery degradation over the years follows the same rate as the PV plant's degradation, 0,5%/year (as a simplification to avoid performing a 25-year simulation). Being aware of the uncertainty of this assumption, this works foresees a possible whole battery system replacement during year 15, to account for degradation losses from the cost side of LCOE calculations. The battery replacement cost in year 15 is estimated at 200 €/kWh, as forecasted by BNEF [55]).

[2] The battery capacity has been sized by means of the MATLAB simulation tool with the criterion of reducing overcharging battery losses to less than ≈1% for the case of *Desired_flat-output_rate = 50%*.

6.2.4.1. Results

The following table summarises some interesting indicators for the two flat-outputs proposed:

	Flat-output = 50%	***Flat-output = 70%***
LCOE (EUR/MWh)	82,9113	81,1004
Overcharging losses (%)	1,05%	0%
Hours with flat-output, Y1	2502 hours	985 hours
Average hours per day with flat-output, Y1	6,85 hours	2,70 hours
% of the year with flat-output, Y1	29%	11%

Table 13. Summarised results for both cases of flat-output response: 50% and 70% of the PV plant nominal capacity.

It can be seen in Table 13 that LCOEs are slightly different despite having the same cost structure (CAPEX and OPEX) since the battery capacity is the same for both cases. The explanation to this fact can be found in overcharging losses (energy burnt during charging because the battery is already 100% charged): when flat-output is at 50%, 1% of the PV output is lost due to overcharging. At 70% of flat-output, this loss is nullified, since most of the PV output is directed to the grid and the battery rests oversized.

In a more general view, it can be observed that both LCOEs are around 30 EUR/MWh higher than the PV plant without a battery. The conclusion is, that from a cost point of view, batteries are not still as competitive as PV plants alone. However, batteries can provide services that must be valued in terms of quality and not of quantity; and maybe in the future these services could be highly rewarded by system operators (e.g. premium tariffs for providing services, allowing energy arbitrage, etc.). In addition, utility-scale battery systems will benefit from economies of scale in Li-ion batteries, induced by the electric vehicle industry, with impressive cost reductions already forecasted.

From a point of view of the flat-output performance itself, it can be observed that the PV+battery system could attain the desired output rate for 2502 hours during the year (50% flat-output case) and 985 hours (70% flat-output), which represents an average of 6,85 and 2,70 hours of flat-output per day respectively. The difference is obvious: a 50% flat-output rate allows the system to have enough energy to both charge the battery while yet attaining the desired rate. However, a 70% flat-output rate makes the system prioritise fulfilling the desired output rate while not enough energy charges the battery.

A visual description of these facts is shown in Figures 25 *a* and *b*, where 3 consecutive days

(3rd, 4th and 5th of April) with outstanding PV production are displayed:

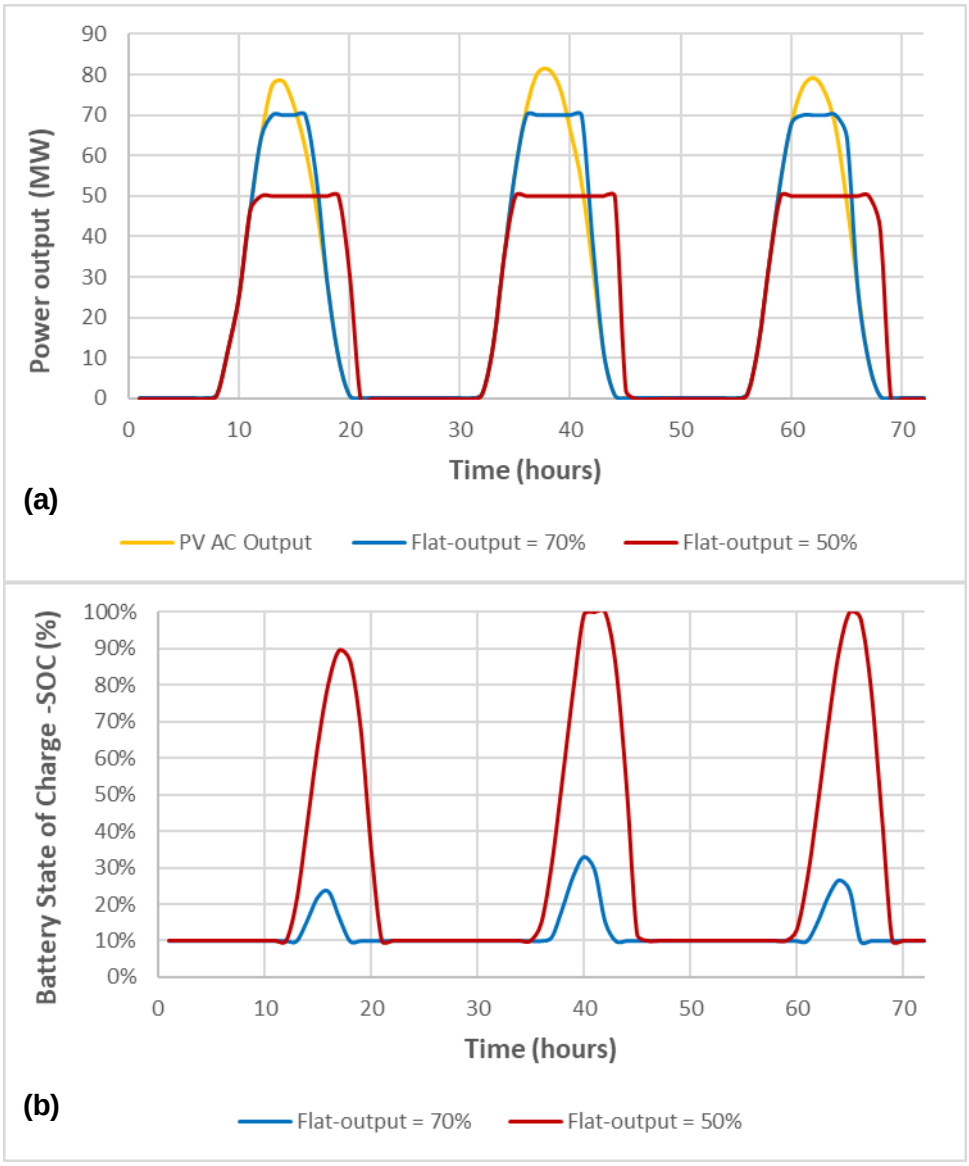

Figure 25. For the 3rd, 4th and 5th of April:

a) Power output of the PV system (yellow) and the flat-output responses: 70% (blue) and 50% (red).

b) Battery state of charge: 70% flat-output case (blue) and 50% flat-output case (red).

Finally, Figure 26 shows the different energy flows that occur in the PV+battery system (for the 4th of April under the 50% flat-output response scenario):

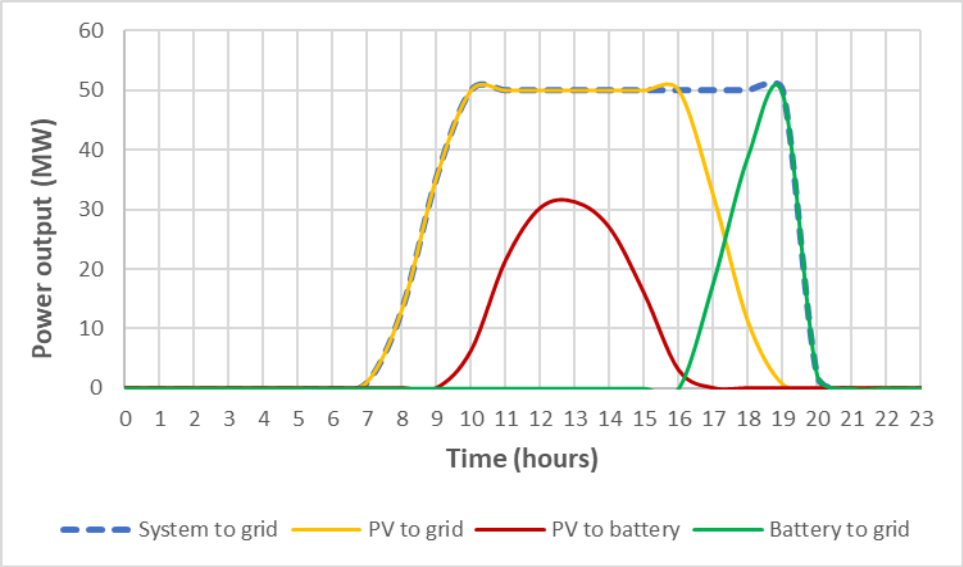

Figure 26. System power flows during the 4th of April: total system to grid (dashed blue line), PV to grid (yellow line), PV to battery (charging, red line) and battery to grid (discharging, green line).

In Figure 26, it can be seen that, during the morning, the PV plant alone satisfies the desired flat-output. Then, at the beginning of the afternoon, the surplus of PV production is stored in the battery. Afterwards, during the evening, the battery starts helping the system to reach the desired flat-output. And from 17:30h, the battery alone starts providing all the output required to the grid during a couple of hours.

6.3. Case studies conclusions

It has been seen that central inverters are, by a small margin, the most cost-effective solution when considering large utility-scale PV plants. However, the intense push in string inverters made by Huawei is starting to pay off: string inverters are already competitive solutions. Optimising DC/AC inverter ratios is a path to reducing PV systems costs.

The inclusion of trackers can increase considerably the energy output, reducing significantly the final LCOE. PV plants with trackers must be carefully designed to minimise self-shading effects. Luckily, tracker manufacturers have already developed back-tracking algorithms.

When considering self-shading in a fixed-axis PV plant, PV developers must optimise their projects by considering techno-economic indicators but also land-use, since it is going to be a concern specially in populated regions like Europe and some regions in South-east Asia.

Batteries are not still a great solution economically speaking, but they will be with the announced cost reductions roadmaps. However, batteries can provide valuable services to the grid, fundamental when considering renewable energies integration.

7. Planning and budget of the project

This section proposes a brief planning and budget for a 100 MW PV power plant in Seville, Spain. Since several case studies have been considered in previous section 6, configuration central 2 (without battery) is selected as the proposed project in this section.

Moreover, since an economic analysis is already provided in the previous section (in the form of the LCOE, the key techno-economic indicator in the energy industry), the budget is going to be the only economic topic of this section.

7.1. Planning of the project

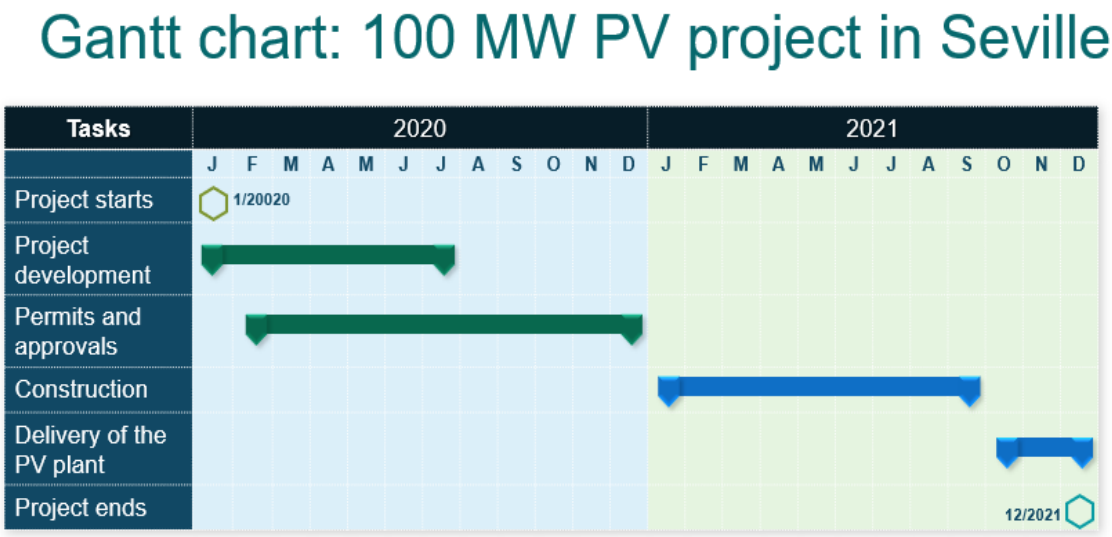

Figure 27. Gantt chart for the development of a PV plant project in Seville. Source: Own.

Figure 27 shows the Gantt chart for the PV project studied. Firstly, it is important to note that there is a previous phase not included in this chart. This phase includes all the project conception and technical documentation made before the project is officially awarded. In utility-scale PV plants, it is common to award projects by public national auctions or tenders, where different companies bid to claim the project. Normally, this previous phase can last for several years.

In our case, Figure 27 project starts when the awarded company assigns the PV plant conception to a project developer or so-called EPC (sometimes the same awarded company is already an EPC). A first stage of **project development** can last around 7 months, including site identification, land acquisition, system design, environmental and social assessments or technology selection.

In parallel, when enough documentation is collected, the **permits and approvals application** to local and national administration starts. This stage can last around 1 year or more depending on the location (11 months in our project). Sometimes, this stage is considered the nightmare of developers and one of the riskiest moments of the project.

Once all the permits and approvals are validated, **construction** can start. Construction includes from site preparation, to mounting structures and modules installation or wiring connections. Construction normally lasts between 6 to 12 months depending on the project characteristics (9 months in our project). Sometimes, certain construction stages can start before receiving all the permits, but it is not considered in this case.

Finally, the **PV plant is delivered**. These includes multiple verifications and check-ups to ensure safety, reliability and performance of the plant. It is estimated in 3 months in this project.

Once all these phases are completed, the PV plant can be brought online. A 2-year timeline has passed to develop this PV project, which is an average time period for projects of this kind.

7.2. Budget of the project

Table 14 shows the budget for the CAPEX of the 100 MW PV project, taxes excluded:

CAPEX item	Unitary cost (EUR/W)	Total cost (M€)
PV modules	0,31 EUR/W_p	31 M€
Central inverters (87 MW_{AC})	0,03 EUR/W_{AC}	2,6 M€
BOS (Balance of System)	0,17 EUR/W_p	17 M€
Other costs (EPC, land, etc.)	0,30 EUR/ W_p	30 M€
TOTAL COSTS	**--**	***80,6 M€***

Table 14. Budget of the 100 MW PV project in millions of euros (M€) and excluding taxes.

The capital expenditures of the project account for 80,6 M€, being the PV modules responsible for more than a third of this amount. This number should be seen as an estimate for similar projects, since budgetary data is commonly non-disclosed by PV developers

The unitary costs (EUR/W) and their sources are originally presented in chapter 6.1.5 (Table 1). As a recall, other costs include the project development costs (EPC costs), the land acquisition costs, civil works or even the developer's margin amongst others.

8. Impacts of the project

In this section, both the environmental and socioeconomic impacts are discussed.

8.1. Environmental impact

8.1.1. Equivalent and avoided CO_2 emissions

There have been many discussions whether PV technologies are as green as they are said to be. Most of these discussions being initiated either by the nuclear lobby or the fossil fuels lobby.

Luckily, experts can easily answer to this controversy by using an impartial tool: the life-cycle assessment (LCA), which is a carefully detailed methodology to assess the environmental impact of a product, process or activity. One of the indicators resulting from this analysis is the carbon footprint, the amount of CO_2 equivalent emissions (greenhouse gases emissions) produced by the product, process or activity studied.

To simplify this assessment in the present work, literature data has been used: a study carried out by D. Yue, F. You, and S. B. Darling (2014) [59] suggests that the carbon footprint for mono c-Si modules manufactured in China and installed in Southern Europe amounts to **2,76 kg CO_2-eq/W_p**. Openly and frankly, this is a worst-case estimate, since it was assessed in 2014 when China's energy mix was much darker and manufacturing processes were less efficient than today. However, for the sake of simplicity and to account for other related emissions of the PV plant (inverters, BOS, etc.), the present work is going to use this estimate.

The 100 MW_p PV plant represents **276.000 t CO_2-eq** in greenhouse gases emissions. Taking configuration central 2 case study, the plant will produce around **3950 GWh** of electricity all over the 25 years. This means an average emission per kWh of electricity production of just **0,07 kg CO_2-eq/kWh**.

On the other hand, the Spanish electricity mix has a 2018 emission factor estimated at **0,321 kg CO_2-eq/kWh** [60], more than 4 times higher than the one obtained by the PV plant. The avoided emissions[3] thanks to the development of the PV plant account almost for **1 Mt CO_2-eq**, which equals to over **16 million of urban trees planted** [61]. In fact, after the 5th year the PV plant has already recovered its initial impact in greenhouse gases emissions.

[3] Avoided emissions are defined as the difference between emissions if generating electricity with the Spanish grid and the emissions of manufacturing the PV modules.

8.1.2. Land-use

Land-use is one of the most impactful results of a PV plant construction. As seen in chapter 6.2.3, considering a GCR of 0,3 (worst case for land-use), 1,67 km^2 of terrain are needed, which equals the surface of a square measuring 1,3 x 1,3 km (the walking distance from Plaça Francesc Macià to Passeig the Gràcia taking l'Avinguda Diagonal in Barcelona).

This land occupied by the PV plant cannot be used for other activities, such as agricultural uses, meaning that some tension could arise from that side. Moreover, if large-scale PV develops heavily in Spain and in Europe, land availability scarcity could occur. However, by relying on high-efficiency PV technologies (more electricity production per area) and with good designing practices, a sustainable PV development in Europe can be ensured.

8.2. Socioeconomic impacts

In general, positive socioeconomic impacts outweigh negative ones. For instance, the local population will benefit socially and economically from the construction phase, because either the human force is going to be local or the displaced workers will enrich the local economy.

Moreover, at a national level, the state is going to be provided with a cheap and green source of energy. Being cheap will allow reducing the Spanish electricity price (in theory, practically this does not usually occur). And being a green source of energy will allow Spain to accomplish its emission reduction goals to fight climate change.

Many other positive socioeconomic impacts can be listed, but also some negative impacts, for instance, the before-mentioned land-use competition or unemployment increase in non-renewable industries. However, negative impacts can be mitigated with adequate policies and adaptation to modern times.

Conclusions

The original MATLAB PV plant simulation tool has been updated and improved with new models, submodels, databases and indicators. Amongst others, three important models have been implemented:

- Tracking system model
- Self-shading model
- Model of the battery (flat-output operation)

The different models added to the code have been validated and used in numerous case studies.

The case studies have been focused in four important topics of interest to PV plant developers:

- Selection between string and central inverters
- Effects of including trackers
- Land-use and PV plant losses due to self-shading between rows
- Effects of including a battery to provide flat-output response

Central inverters still represent the most cost-effective solution, but the string inverter push is intense and starts to pay off. DC/AC inverter ratios play an important role in PV plant designing.

Tracker devices usually increase energy yield while reducing LCOE by simply adding a small add-on in CAPEX.

A dilemma exists between reducing self-shading losses and reducing land-use: self-shading losses increase as land-use is reduced.

Batteries will play a key role in future power grids, providing services like the one studied in this project (flat-output response). However, batteries are not still as profitable as PV systems alone. Cost reduction roadmaps will enhance battery projects profitability.

Finally, it has been seen that PV plants can be developed relatively quick (periods up to 2 years) and their positive impacts largely outweighs their negative ones.

The work in this project could be extended by others, for example, by including a self-shading model when tracking is considered. This will allow analysing in detail trackers performance. Furthermore, with a valid tracking self-shading model, designing and optimising backtracking algorithms will be possible.

Acknowledgments

Primer de tot, vull agrair a la direcció i al personal (docent i no docent) de l'ETSEIB per aquests anys de formació que s'acaben amb aquestes línies. Han estat gairebé 8 anys, un grau i dos màsters i la possibilitat de marxar a l'estranger a estudiar, treballar i viure. És a l'estranger on un es dóna compte de l'excelent nivell de formació i sobretot d'aquesta multidisciplinaritat i transversalitat que ens porten a adaptar-nos a diferents condicions i reptes.

També vull agrair al meu tutor, el professor Oriol Gomis, per deixar-me participar en el desenvolupament d'aquest programa MATLAB començat per un altre estudiant, en Gabriele Catalano, que des d'aquí aprofito per agrair-li i felicitar-lo pel seu gran treball en la creació del programa original.

No vull oblidar-me de la meva familia (pares, germana, avis, tiets, cosins) que han estat "suportant" i "aguantant" tots aquests anys fins al dia d'avui. Especialment els meus pares, qui crec que finalment estaran satisfets del resultat d'aquests 8 darrers anys.

Et finalement à toi Julie (et à ta famille également !), pour me soutenir et m'encourager pendant ces derniers mois d'intense travail sur ma thèse.

Bibliography

References

[1] Catalano, G. (2018). Development of a model to simulate solar PV plants in MATLAB with a study on the effects of undersizing the inverter. MSc Thesis. UPC, Barcelona, Spain. [ONLINE] Available at:

https://upcommons.upc.edu/handle/2117/127357 (Accessed April 1, 2019).

[2] P. Gilman, A. Dobos, N. DiOrio, J. Freeman, S. Janzou, and D. Ryberg. SAM Photovoltaic Model Technical Reference Update (2018). Colorado, USA. [ONLINE] Available at:

https://www.nrel.gov/docs/fy18osti/67399.pdf (Accessed April 1, 2019).

[3] PVsyst (2018). First Solar Spectral Correction. Geneva, Switzerland. [ONLINE] Available at:

http://files.pvsyst.com/help/firstsolar-spectral-correction.htm (Accessed April 1, 2019).

[4] First Solar (2017). Module Characterization: Spectral Response of FS Series PV Modules. [ONLINE] Available at:

http://www.firstsolar.com/en-EMEA/-/media/First-Solar/Technical-Documents/Series-4-Energy-Prediction/Spectral-Response-of-FS-Series-PV-Modules.ashx?la=en
(Accessed April 1, 2019).

[5] K. Jäger, O. Isabella, A. Smets, R. van Swaaij, M. Zeman (2014). Solar Energy - Fundamentals, Technology, and Systems. Delft University of Technology. Netherlands.

[6] M.A. Green (1995). Silicon Solar Cells: Advanced Principles and Practice. Bridge Printery, Sydney, Australia.

[7] PVmagazine (2019). Global solar demand reached 104 GW in 2018. [ONLINE] Available at:

https://www.pv-magazine.com/2019/03/06/global-solar-demand-reached-104-gw-in-2018/ (Accessed April 1, 2019).

[8] PVTECH (2018). Global solar market hit 98.9GW in 2017 - SolarPower Europe. [ONLINE] Available at:

https://www.pv-tech.org/news/global-solar-market-hit-98.9-gw-in-2017-solarpower-europe (Accessed April 1, 2019).

[9] PVmagazine (2019). China installed 44.1 GW of solar in 2018, according to official NEA data. [ONLINE] Available at:

https://www.pv-magazine.com/2019/01/21/china-installed-44-1-gw-of-solar-in-2018-according-to-official-nea-data/ (Accessed April 1, 2019).

[10] PVmagazine (2018). BNEF expects 34% fall in PV module prices in 2018. [ONLINE] Available at:

https://www.pv-magazine.com/2018/06/05/bnef-expects-34-fall-in-pv-module-prices-in-2018/ (Accessed April 1, 2019).

[11] PVmagazine (2018). EU officially ends MIP for Chinese solar imports. [ONLINE] Available at:

https://www.pv-magazine.com/2018/08/31/eu-ends-mip-against-chinese/ (Accessed April 1, 2019).

[12] IEA PVPS, (2018). Trends 2018 in photovoltaic applications. International Energy Agency (IEA), France. [ONLINE] Available at:

http://www.iea-pvps.org/fileadmin/dam/public/report/statistics/2018_iea-pvps_report_2018.pdf (Accessed April 1, 2019).

[13] LAZARD (2018). Lazard's Levelized Cost of Energy Analysis. New York, USA. [ONLINE] Available at:

https://www.lazard.com/media/450784/lazards-levelized-cost-of-energy-version-120-vfinal.pdf (Accessed April 1, 2019).

[14] PVmagazine (2018). Solar, wind cheapest source of new generation in major economies – report. [ONLINE] Available at: https://www.pv-magazine.com/2018/11/19/solar-wind-cheapest-source-of-new-generation-in-major-economies-report/ (Accessed April 1, 2019).

[15] BNEF (2018). 2Q 2018 Global PV Market Outlook. Bloomberg New Energy Finance (BNEF). [ONLINE] Available at: Subscription Service (Accessed May 9, 2018).

[16] Fraunhofer ISE (2018). Photovoltaics report. Fraunhofer Institute for Solar Energy Systems, ISE, Germany. [ONLINE] Available at:

https://www.ise.fraunhofer.de/content/dam/ise/de/documents/publications/studies/Photovoltaics-Report.pdf (Accessed April 1, 2019).

[17] M.A. Green (2015). The Passivated Emitter and (PERC): From conception to mass production. University of New South Wales (UNSW). Sydney, Australia. [ONLINE] Available at: https://www.sciencedirect.com/science/article/pii/S0927024815003244 (Accessed April 1, 2019).

[18] M. A. Green, Y. Hishikawa, E. D. Dunlop, D. H. Levi, J. Hohl-Ebinger, and A. W. Y. Ho-Baillie, "Solar cell efficiency tables (version 53)," Prog. Photovoltaics Res. Appl., vol. 27, no. 1, pp. 3–12, 2018.

[19] W. Shockley, H.J. Queisser (1961). Detailed Balance Limit of Efficiency of p-n Junction Solar Cells. Journal of Applied Physics 32, 510.

[20] ITRPV, VDMA (2019). International Technology Roadmap for Photovoltaic (ITRPV): 2018 Results. [ONLINE] Available at: https://itrpv.vdma.org/ (Accessed April 1, 2019).

[21] First Solar (2019). CdTe Module Manufacturer. Arizona, USA. [ONLINE] Available at: http://www.firstsolar.com/ (Accessed April 1, 2019).

[22] First Solar (2017). First Solar's energy advantage in Indian climatic conditions. Arizona, USA. [ONLINE] Available at: http://www.firstsolar.com/-/media/First-Solar/Knowledge-Center/Technology-Advantage/Renewable-Watch---Case-Study.ashx (Accessed April 1, 2019).

[23] Solar Frontier (2019). CIGS Module Manufacturer. Tokyo, Japan. [ONLINE] Available at: http://www.solar-frontier.com/eng/ (Accessed April 1, 2019).

[24] PV magazine (2017). The weekend read: CIGS is back, back again. [ONLINE] Available at: https://www.pv-magazine.com/2018/07/21/the-weekend-read-cigs-is-back-back-again/ (Accessed April 1, 2019).

[25] PV magazine (2017). Momentum builds for HJT. [ONLINE] Available at: https://www.pv-magazine.com/magazine-archive/momentum-builds-for-hjt/ (Accessed April 1, 2019).

[26] Renewable Market Watch (2018). Renaissance for Solar Photovoltaic (PV) Market in Spain. [ONLINE] Available at:

http://renewablemarketwatch.com/news-analysis/265-renaissance-for-solar-photovoltaic-pv-market-in-spain (Accessed April 1, 2019).

[27] PV magazine (2017). Spain loses its first renewable energy case in international courts. [ONLINE] Available at: https://www.pv-magazine.com/2017/05/05/spain-loses-its-first-renewable-energy-case-in-international-courts/ (Accessed April 1, 2019).

[28] PV magazine (2019). Spain hits 5 GW milestone. [ONLINE] Available at:

https://www.pv-magazine.com/2019/02/05/spain-hits-5-gw-milestone/ (Accessed April 1, 2019).

[29] SolarPower Europe (2019). Spain's solar market is reignited. [ONLINE] Available at:

http://www.solarpowereurope.org/spains-solar-market-gives-grounds-for-optimism/ (Accessed April 1, 2019).

[30] PV magazine (2018). Four key solar takeaways from Spain's Genera 2018. [ONLINE] Available at:

https://www.pv-magazine.com/2018/06/15/four-key-solar-takeaways-from-spains-genera-2018/ (Accessed April 1, 2019).

[31] PV magazine (2019). "Spain is the hottest PPA market in the world, but auctions are necessary". [ONLINE] Available at:

https://www.pv-magazine.com/2019/02/21/spain-is-the-hottest-ppa-market-in-the-world-but-auctions-are-necessary/ (Accessed April 1, 2019).

[32] Wikipedia (2019). El Dorado. [ONLINE] Available at:

https://en.wikipedia.org/wiki/El_Dorado (Accessed April 1, 2019).

[33] PV magazine (2018). "Flow battery breakthrough?. [ONLINE] Available at:

https://www.pv-magazine.com/magazine-archive/flow-battery-breakthrough/ (Accessed April 1, 2019).

[34] H. Cho, A. Smith, R. Luck, P.J. Mago (2017). Transient Uncertainty Analysis in Solar Thermal System Modeling. Missipi State University, USA.

[35] PVsyst (2019). Soiling loss. [ONLINE] Available at:

http://files.pvsyst.com/help/soiling_loss.htm (Accessed April 1, 2019).

[36] Sandia National Laboratories (2019). Sandia Inverter Model. [ONLINE] Available at:

https://pvpmc.sandia.gov/modeling-steps/dc-to-ac-conversion/sandia-inverter-model/ (Accessed April 1, 2019).

[37] PV magazine USA (2017). NEXTracker leads global PV tracker market. [ONLINE] Available at:

https://pv-magazine-usa.com/2017/03/30/nextracker-leads-global-pv-tracker-market/ (Accessed April 1, 2019).

[38] BNEF (2017). Tracking the Sun Has a Bright Future. Bloomberg New Energy Finance (BNEF). [ONLINE] Available at: Subscription Service (Accessed May 9, 2018).

[39] W. F. Marion and A. P. Dobos (2013). Rotation Angle for the Optimum Tracking of One-Axis Trackers. NREL, Colorado, USA.

[40] C. Deline, A. Dobos, S.Janzou, J. Meydbray, M. Donovan (2013). A simplified model of uniform shading in large photovoltaic arrays. NREL, Colorado, USA.

[41] REC Group (2019). REC N-Peak. [ONLINE] Available at:

https://www.recgroup.com/en/products/rec-n-peak-en (Accessed April 1, 2019).

[42] J. Appelbaum, J. Bany (1979). Shadow effect of adjacent solar collectors in large scale systems. Tel-Aviv University, Israel.

[43] M. De Prada-Gil, J.L. Domínguez-García, L. Trilla, O. Gomis-Bellmunt (2016). Technical and economic comparison of various electrical collection grid configurations for large photovoltaic power plants. IREC/CITCEA-UPC, Barcelona, Spain.

[44] W. De Soto, S.A. Klein, W.A. Beckman (2004). Improvement and validation of a model for photovoltaic array performance. Solar Energy Laboratory, University of Wisconsin-Madison, USA.

[45] SINOVOLTAICS (2015). PID & LID: Devastating Phenomena for PV plants. [ONLINE] Available at:

https://sinovoltaics.com/quality-control/pid-lid-devastating-phenomena-pv-plants/ (Accessed April 1, 2019).

[46] Go Solar California (2019). Energy Commission's Solar Equipment Lists. California,

USA. [ONLINE] Available at:

https://www.gosolarcalifornia.ca.gov/equipment/index.php (Accessed April 1, 2019).

[47] SolarPower Europe (2018). O&M Best Practices Guidelines 3.0. [ONLINE] Available at:

http://www.solarpowereurope.org/wp-content/uploads/2018/12/OM-Best-Practices-Guidelines-V3.0.pdf (Accessed April 1, 2019).

[48] PVTECH (2019). Top 10 module suppliers in 2018. [ONLINE] Available at:

https://www.pv-tech.org/editors-blog/top-10-solar-module-suppliers-in-2018 (Accessed April 2, 2019).

[49] JA Solar (2019). 72-Cell Mono PERC Module- JAM72S01/PR. Shanghai, China. [ONLINE] Available at:

http://www.jasolar.com/index.php?m=content&c=index&a=show&catid=84&id=9 (Accessed April 2, 2019).

[50] HUAWEI (2019). Smart PV String Inverters. Shenzhen, China. [ONLINE] Available at:

http://solar.huawei.com/eu/products (Accessed April 2, 2019).

[51] SMA (2019). SUNNY CENTRAL 2200 / 2475 / 2500-EV / 2750-EV / 3000-EV. Niestetal, Germany. [ONLINE] Available at:

https://www.sma.de/en/products/solarinverters/sunny-central-2200-2475-2500-ev-2750-ev-3000-ev.html (Accessed April 2, 2019).

[52] C. Kost, J. N. Mayer, J. Thomsen, N. Hartmann, C. Senkpiel, S. Philipps, S. Nold, S. Lude, N. Saad, T. Schlegl (2013). Levelized Cost of Electricity Renewable Energy Technologies Study. Fraunhofer Institute for Solar Energy Systems ISE, Germany.

[53] IRENA (2018). Renewable Power Generation Costs in 2017. International Renewable Energy Agency (IRENA), Abu Dhabi. [ONLINE] Available at:

http://www.irena.org/publications/2018/Jan/Renewable-power-generation-costs-in-2017 (Accessed April 4, 2018).

[54] BNEF (2018). 2018 Solar Inverter Market Outlook. Bloomberg New Energy Finance (BNEF). [ONLINE] Available at: Subscription Service (Accessed May 9, 2018).

[55] BNEF (2018). New Energy Outlook 2018. Bloomberg New Energy Finance (BNEF).

[ONLINE] Available at: Subscription Service (Accessed June 14, 2018).

[56] BNEF (2018). PV O&M 2017: Providers Push Their Limits for Lower Prices. Bloomberg New Energy Finance (BNEF). [ONLINE] Available at: Subscription Service (Accessed May 9, 2018).

[57] PVsyst (2018). How to define the "Mismatch Loss" parameter? [ONLINE] Available at:

https://forum.pvsyst.com/viewtopic.php?t=47 (Accessed April 4, 2019).

[58] PVsyst (2018). LID loss. [ONLINE] Available at:

http://files.pvsyst.com/help/lid_loss.htm (Accessed April 4, 2019).

[59] D. Yue, F. You, and S. B. Darling, “Domestic and overseas manufacturing scenarios of silicon-based photovoltaics: Life cycle energy and environmental comparative analysis,” Sol. Energy, vol. 105, pp. 669–678, 2014.

[60] The Catalan Office for Climate Change (OCCC) (2019). Emission factors related to electrical energy: the electrical mix. Barcelona, Spain. [ONLINE] Available at:

http://canviclimatic.gencat.cat/en/redueix_emissions/com-calcular-emissions-de-geh/factors_demissio_associats_a_lenergia/ (Accessed April 18, 2019).

[61] United States Environmental Protection Agency (EPA) (2019). Greenhouse Gas Equivalencies Calculator. United States. [ONLINE] Available at:

https://www.epa.gov/energy/greenhouse-gas-equivalencies-calculator (Accessed April 18, 2019).